LUND UNIVERSITY

X-LINKED RETINOSCHISIS ELECTROPHYSIOLOGY, MOLECULAR GENETICS AND TREATMENT

Kjellström, Sten

2010

X-LINKED RETINOSCHISIS

ELECTROPHYSIOLOGY, MOLECULAR GENETICS AND TREATMENT

Sten Kjellström, MD

LUND UNIVERSITY
Faculty of Medicine

Department of Ophthalmology
Lund University
2010

Scan me ☺

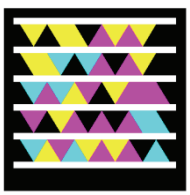

Doctoral Dissertation 2010
Department of Ophthalmology
Lund University, Sweden

ISSN 1652-8220
ISBN 978-91-86443-64-1
Lund University, Faculty of Medicine Doctoral Dissertation Series 2010:49

Printed by Media-Tryck, Lund University, 2010

YES WE CAN
Barack Obama

To my mother

Contents

Abbreviations

XLRS	X-linked retinoschisis
RS1	Human retinoschisin protein
Rs1	Mouse retinoschisin protein
RS1	Human retinoschisin gene
Rs1	Mouse retinoschisin gene
Rs1-KO	Retinoschisin knockout mouse
Rs1$^{-/y}$	Retinoschisin knockout mouse
Rs1h	Mouse retinoschisin gene (old nomenclature)
Rs1h-KO	Retinoschisin knockout mouse (old nomenclature)
WT	Wild type
ERG	Electroretinogram
mfERG	Multifocal electroretinogram
OCT	Ocular coherence tomography
RP	Retinitis pigmentosa
BCVA	Best corrected visual acuity
VF	Visual field
AAV	Adeno-associated virus
GCL	Ganglion cell layer
IPL	Inner plexiform layer
INL	Inner nuclear layer
OPL	Outer plexiform layer
ONL	Outer nuclear layer
RPE	Retinal pigment epithelium

List of papers

This thesis is based upon the following papers, which will be referred to in the text by their roman numerals.

I. Zeng Y., Takada Y., **Kjellstrom S.**, Hiriyanna K., Tanikawa A., Wawrousek E., Smaoui N., Caruso R., Bush R. A. and Sieving P. A. RS-1 Gene Delivery to an Adult Rs1h Knockout Mouse Model Restores ERG b-Wave with Reversal of the Electronegative Waveform of X-Linked Retinoschisis. *Invest Ophthalmol Vis Sci* 2004;45:3279-3285.

II. **Kjellstrom S.**, Bush R.A., Zeng Y., Takada Y., Sieving P.A. Retinoschisin gene therapy and natural history in the *Rs1h*-KO mouse: long-term rescue from retinal degeneration. *Invest Ophthalmol Vis Sci* 2007;48:3837-3845.

III. Luna G, **Kjellstrom S.**, Verardo M.R., Lewis G.P., Byun J., Sieving P.A. and Fisher S.K. The effects of transient retinal detachment on cavity size and glial and neural remodeling in a mouse model of X-linked retinoschisis. *Invest Ophthalmol Vis Sci* 2009;50:3977-3984.

IV. **Kjellström S.**, Vijayasarathy C., Ponjavic V., Sieving P.A. and Andréasson S. Long-term 12 year follow-up of X-linked congenital retinoschisis. *Ophthalmic Genetics,* In Press

V. **Kjellström S.**, Ghosh F. Holm K., and Andréasson S. Alteration of vitreal RS1-protein level in human primary retinal detachment. *Manuscript*

Introduction

General Background

Vision is one of the most fundamental of our five senses, and it is of a tragedy when blindness takes this modality from us. The eye is a complex organ, and all parts of the eye are of importance for perceiving a good image. The neuro-retina, being a part of the central nervous system, is vital for vision as it gets direct stimulation from the outside in the form of light and converts it to a neuronal signal. With the retina being a complex and delicate structure, there are many ways the processing and signaling can fail after the photoreceptor has been stimulated by a single photon. In young people in the western world, hereditary retinal degeneration is the most frequent reason for severe visual handicap. We are beginning to understand the pathophysiology behind most of these disorders but we have yet to design a functionally successful treatment. With the fast progress in the field of molecular genetics we are now approaching viable treatments in at least some of these genetic disorders.

Retinal morphology

The retina is located at the back of the human eye and has two types of photoreceptors, cones and rods (Fig 1). In an adult retina there are approximately 7 million cones located mainly in the fovea, the central part of the retina that is responsible for the high detailed daylight color photopic vision. The rods, about 75-150 million, mediate night vision (scotopic vision) and are abundant throughout the retina except for the very central part of the fovea (Osterberg 1935). When a photon is absorbed by a chromophore in the outer segments of a photoreceptor, a cascade of enzymatic reactions is started leading to polarity change of the photoreceptor, i.e. a hyperpolarization of the cell. This cascade, known as the photo transduction, triggers signals that are transmitted to the ganglion cells which forms the optic nerve. Between the ganglion cell layer and the photoreceptors there are two layers where synaptic

contacts are made, the outer plexiform layer (OPL) and the inner plexiform layer (IPL). In the OPL, the rods and cones connect to the vertically running bipolar cells and the horizontally oriented horizontal cells. In the IPL, the bipolar cells and retinal ganglion cells form synapses which are modulated by the horizontally oriented amacrine cells. The slender photoreceptors do not contain everything to maintain their cellular function internally, and they depend on the retinal pigment epithelium (RPE) for the isomerization of all-trans-retinol to 11-cis retinal, the vitamin A cycle that is crucial in phototransduction. The RPE, which is located in the distal part of the retina, is also involved in the phagocytosis of the photoreceptor outer segment discs to help maintain structural integrity of these cells. The only cells in the retina spanning the entire thickness of the tissue, thus connecting the inner with the outer retinal surface, are the Müller cells, which constitute the dominant glial cell type in the retina.

Because of the morphological arrangement with the ganglion cells lying innermost in the retina and the photon absorbing photoreceptors in the distal part, photons must first pass through and around the ganglion cells and through the full thickness of the retina before light is detected. Hence it is of great importance for good vision to maintain the structural integrity of the retina and of the previous structures in the eye that photons pass on their way to the retina.

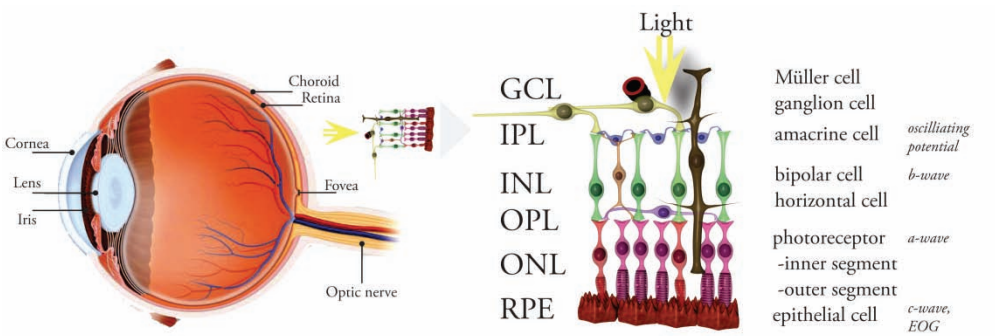

Figure 1. Anatomy of the eye and retina. GCL-ganglion cell layer, IPL-inner plexiform layer, INL-inner nuclear layer, OPL-outer plexiform layer, ONL-outer nuclear layer, RPE-retinal pigment epithelium layer. On the right: ERG signals correlated with origin. (Courtesy of Dr Fredrik Ghosh, Dep. of Ophthalmology, Lund, reproduced and modified with permission)

Human Juvenile X-linked Retinoschisis Disease

History

Haas first described the clinical features of X-linked juvenile retinoschisis (XLRS) as early as 1898(Haas 1898). The disorder has been known by many other names such as vitreous veils, congenital vascular veils in the vitreous and congenital cystic retinal detachment. In 1913 it was first described as an x-linked trait (Pagenstecher 1913) and in 1953 Jager introduced the term retinoschisis, schisis being the Greek word for splitting(Jager 1953)The responsible gene was identified 1997 by Sauer et al(Sauer, Gehrig et al. 1997).

Molecular Genetics

XLRS is a genetic X-linked recessive retinal disease that affects 1:5000 to 1:25000 males worldwide with the highest prevalence reported in Finland (Forsius, Krause et al. 1973; de la Chapelle, Harper et al. 1994) and is one of the more common causes of vision loss from retinal degeneration affecting young men (George, Yates et al. 1995). XLRS is a monogenic trait caused by mutations in the RS1 gene (Sauer, Gehrig et al. 1997; The Retinoschisis 1998) in Xp22.1 and is organized into six separate exons interspaced by five introns (Fig 2).

Currently, more than 170 disease-causing mutations have been identified in the RS1 gene (RetinoschisisDB; http://www. dmd.nl/rs/index.html/ provided in the public domain by Leiden University Medical Center, Leiden, The Netherlands), with missense mutations being the greater part followed by frame-shift, nonsense, and point mutations, deletions, and insertions. Patients with XLRS exhibit a marked heterogeneity in disease severity and progression, and, so far, no strict correlations between genotype and clinical phenotype have convincingly been identified(Roesch, Ewing et al. 1998; Bradshaw, George et al. 1999; Hiriyanna, Bingham et al. 1999; Sieving, Bingham et al. 1999; Eksandh, Ponjavic et al. 2000; Shinoda, Ishida et al. 2000; Hotta, Nakamura et al. 2001; Pimenides, George et al. 2005; Lesch, Szabo et al. 2008). Currently, there is no standardized grading of the disease severity in XLRS. The heterogeneity in involvement of the fovea, a small region with the highest concentration of cone photoreceptors in the retina responsible for our

most accurate visual acuity, is possibly of more importance to the visual acuity outcome than the actual genotype.

The *Rs1* gene product, retinoschisin, is expressed in the retina (Takada, Fariss et al. 2004) and in the pineal gland (Takada, Fariss et al. 2006). It is a 224 amino acid protein of 24kDa that contains an evolutionarily conserved discoidin domain implicated in cell adhesion and signaling (Vogel 1999) (Fig 2). Retinoschisin is predicted to serve as an adhesive protein in maintaining structural and functional integrity of the retina (Wu, Wong et al. 2005), where it is predominantly expressed by the photoreceptor and bipolar cells and localized along the surface of photoreceptors inner segment, outer nuclear and outer plexiform layers of the outer retina and the surface of bipolar cells in the inner retina.

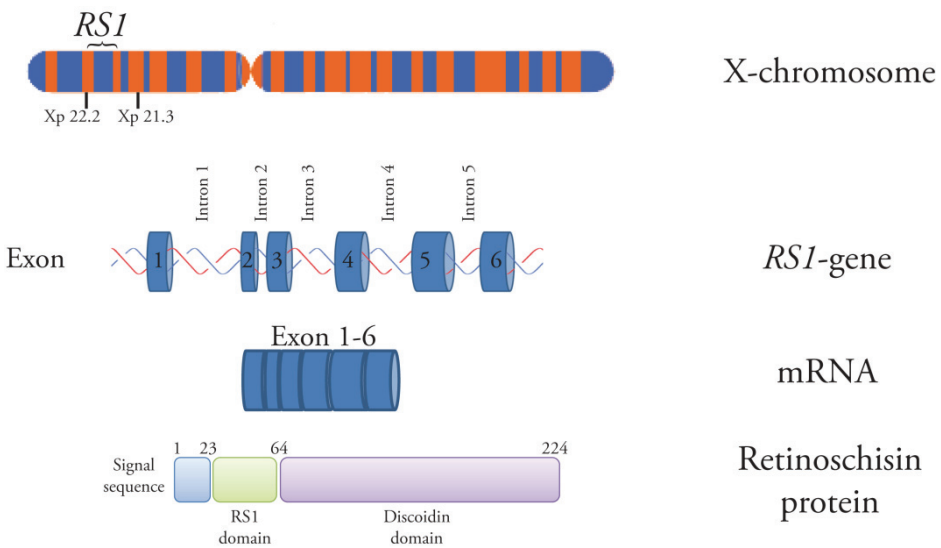

Figure 2. Localization of the Retinoschisin gene *RS1* on the human X-chromosome and a schematic structure of the *RS1* gene and its mRNA and protein products. The functional domains of retinoschisin protein RS1: lead sequence, RS1 and the discoidin domain.

Clinical presentation

Although the disease is congenital, most affected males are diagnosed about the time they reach school age because of poor vision and reading difficulties. The condition manifests clinically with cystic changes in the macula affecting visual acuity which is frequently reduced to Snellen 0.2 – 0.4 (20/100 - 20/50) but can be in the range from light perception to 0.8 (20/25) (Fig. 3). In younger patients a high bullous schisis can often be seen centrally (George, Yates et al. 1995). Later on, a lower foveal schisis is frequently seen as a spoke-wheel pattern with folds radiating out from the center and often a golden-white fundus reflex, mizuo reflex, due to extracellular changes in potassium concentration (de Jong, Zrenner et al. 1991). In some severe cases with nystagmus, bilateral bullous schisis cavities and retinal detachment, the affected males are diagnosed already in the first months of life (George, Yates et al. 1995).

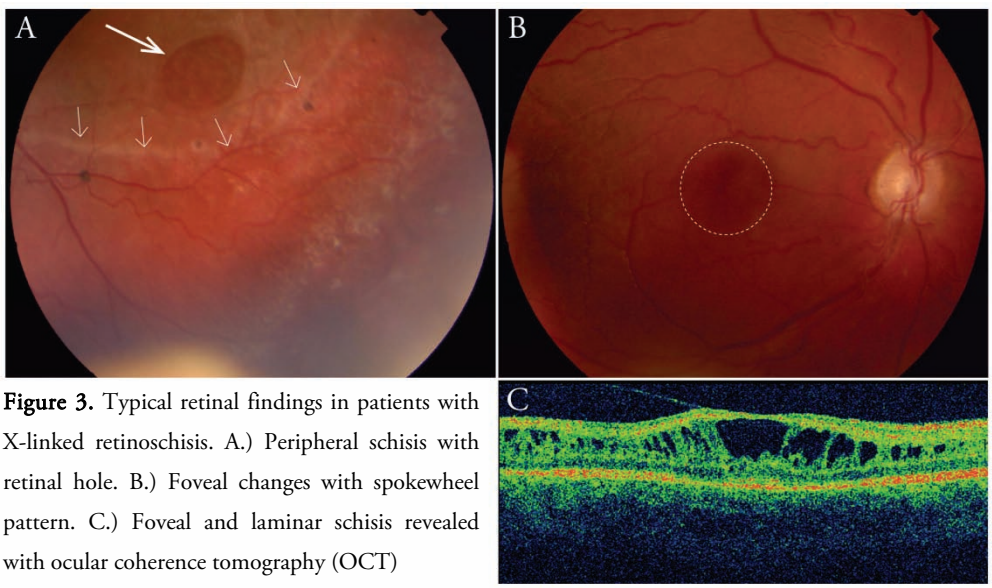

Figure 3. Typical retinal findings in patients with X-linked retinoschisis. A.) Peripheral schisis with retinal hole. B.) Foveal changes with spokewheel pattern. C.) Foveal and laminar schisis revealed with ocular coherence tomography (OCT)

Clinical retinoschisis changes extend into the peripheral retina and cause lamellar splitting through multiple retinal levels, both in the nerve fiber layer at the retinal surface and also deeper in the retina. Peripheral retinoschisis occurs most commonly in the infero-temporal retina (Eksandh, Ponjavic et al. 2000). The clinical literature indicates that about half of affected males have

peripheral retinoschisis (George, Yates et al. 1995) and that these may lead to retinal lamellar holes with full thickness retinal detachment. The introduction of optical coherence tomography (OCT) has increased the clinical sensitivity for detection (Prenner, Capone et al. 2006), and a majority of XLRS males are found to have peripheral retinal involvement with schisis formations (Gerth, Zawadzki et al. 2008). Compared to the general population, affected males are more prone to retinal detachment (RD) (10 vs. 0.01%, respectively) (Kellner, Brummer et al.; Sasaki, Ideta et al. 1995). These detachments are also often difficult to surgically reattach, making the postoperative outcome unfavorable (Regillo, Tasman et al. 1993; Rosenfeld, Flynn et al. 1998). Other complications include vitreous hemorrhage.

The clinical phenotype of XLRS is quite variable in the age and severity of clinical presentation and in the extent of peripheral retinal pathology (Tantri, Vrabec et al. 2004). Visual deterioration, principally visual acuity loss, typically progresses during the first two decades of life. XLRS affected men often barely qualify for a driver's license (Sweden 0.5 Snellen). There is slow progression of severity into the fifth and sixth decades with an early onset age related macular degeneration that commonly causes additional visual failure (Kellner, Brummer et al. 1990; Eksandh, Ponjavic et al. 2000). XLRS patients over the age of 50 years frequently have macular pigmentary changes and/or retinal pigment epithelial (RPE) atrophy. The older age consequences have not been fully described, but in our clinical experience, visual failure can become profound even without complicating factors such as retinal detachment or vitreous hemorrhage, implicating a progressive failure and loss of retinal cells and function.

Female carriers of an *RS1* gene mutation on one allele i.e. heterozygote, are in general asymptomatic with normal visual acuity and normal full-field electroretinogram (ERG) responses. Recently, subtle abnormalities in multifocal-ERG (mfERG) amplitude and timing at a few retinal loci have been described in a minority of carrier women (Kim, Seiple et al. 2007). There is one description in the literature where females have typical XLRS findings. In this case, they were offspring of an affected man and a carrier woman in the context of a consanguineous family (Rodriguez, Rodriguez et al. 2005)

In other X-linked retinal diseases such as X-linked retinitis pigmentosa and choroideremia, carrier women frequently show clinical abnormalities in retinal pigmentation or full-field electroretinography (Sieving, Niffenegger et al. 1986). Sparing of the XLRS heterozygous carrier females is likely due to the nature of the product of the *RS1* gene, the protein retinoschisin. Evidence indicates that retinoschisin is a secreted protein, and even a reduced amount of protein synthesized in the retina of a female carrier appears to fulfill its function as a putative adhesion/stabilization molecule. As a consequence of random inactivation of one X chromosome in female XX cells, i.e. lyonization, the retina of XLRS carrier women will contain a mixture of both normal and mutant gene products. Saldana et al. recently described a young female heterozygous for a *RS1* gene mutation, with clinical features of XLRS (Saldana, Thompson et al. 2007). In this case, it is believed to be caused by a skewed X inactivation leaving areas of the retina without retinoschisin. The absence of clinical disease in carrier women implies that the replacement level of protein expression need not reach that found in normal retinas to promote substantial therapeutic function.

Function

The full-field electrogram (ERG) is a widely used clinical and research electrophysiology test of retinal function in both humans and animals. In all living cells there are gradients of ions across membranes. These give rise to currents that can be measured, e.g. electrocardiogram (ECG) and electroencephalogram (EEG). Holmgren (Holmgren 1865) showed as early as 1865 that an alteration in electrical potential occurred when light fell on the retina, and Dewar recorded a light-evoked electrical response, the ERG, from humans for the first time 1877 (Dewar 1877). In 1933 Ragnar Granit published his first detailed study of different waveforms constituting an ERG recording, and this, slightly modified, still remains the basis for our understanding of the ERG (Granit 1933). For this he was awarded the Nobel Prize for Physiology and Medicine in 1967.

In dark adapted condition, when no light reaches the photoreceptors, there is a current across the photoreceptors, the dark current. When photons activate the phototransduction cascade by altering the state of membrane bound rhodopsin the photoreceptor closes its sodium channels and becomes

hyperpolarized. This change in polarity of the photoreceptor decreases the release of synaptic transmitter substance and activates the bipolar cells which transmit the signal to the ganglion cells whose axons forms the optic nerve. Horizontal and amacrine cells modulate these synaptic connections by transmitting information from adjacent retinal cells.

Electrodes are placed on the cornea and the entire retina is illuminated. The visual stimuli changes the membrane potentials over time in a large number of excitable cells, and because of the parallel alignment of the photoreceptors, this gives rise to a measurable radial extracellular current flowing away from the inner nuclear layer towards the pigment epithelium. By changing the conditions under which the ERG is recorded as to the wavelength, intensity, frequency, and duration of the light stimulus, in addition to the state of light/dark adaptation of the patient, the function of the different retinal cells can be evaluated individually.

Rod function is investigated following dark adaptation (scotopic condition) for least 20 min using dim stimulus flashes. The mixed rod-cone function is also studied under this dark scotopic condition using brighter white stimuli. Pure cone derived recordings can be achieved by light adapting the retina for at least ten minutes with bright background light (photopic condition). After the rod system is desensitized by this background light the cone function can be analyzed using flashes of bright light. Another way of separating the electrical signals from rods and cones is to use flickering light. Bright light flicker stimulation separates cones from rods since the fusion frequency is much lower for rods than for cones. The fusion frequency is the frequency of light stimulation using a specific intensity of light where the eye can no longer discriminate flickering light as single flashes but perceives a steady light.

The major components of the scotopic bright full-field ERG response are the cornea-negative a-wave and the cornea-positive b-wave (Fig 4). The scotopic a-wave reflects primarily the rod photoreceptor light response (Penn and Hagins 1969; Breton, Schueller et al. 1994), and the b-wave reflects post-synaptic bipolar cell activity, albeit driven by photoreceptor input.(Newman and Odette 1984; Stockton and Slaughter 1989; Xu and Karwoski 1994; Robson and Frishman 1995) The ratio between the second order neuron response, i.e.

from bipolar cells, and the first order neuron response i.e. from photoreceptors is the b-wave/a-wave ratio. This is suggested to be a measurement of synaptic function between the light sensing photoreceptors and the light-processing inner neuronal cell layers (Fig. 1). The flicker ERG recordings using high intensity 30Hz flickering light is mainly cone photoreceptor mediated, although other retinal cells, such as bipolar cells, contribute to a varying degree depending frequency and duration of the light flashes. The amplitudes of the a- and b-wave are measured in microvolt (μV) while the time to peak (implicit time) is measured in milliseconds (ms). The amplitude and timing of the a-wave is measured from the baseline to the a-wave through. Amplitude and implicit time of the b-wave is measured from the a-wave though to the b-wave peak

A typical scotopic full-field ERG finding in XLRS patients is a reduction of the b-wave response disproportionate to the a-wave (Peachey, Fishman et al. 1987), i.e. a decrease in b/a-wave ratio, indicating abnormal retinal signaling (Fig. 4). This is believed to be due to splitting within the retinal layer, between the photoreceptor cell layer and inner neuronal cell layers, which would impair visual signal transduction. Furthermore, there is often a delay in the 30Hz flicker ERG implicit time (Deutman 1971; Kellner, Brummer et al. 1990; Eksandh, Ponjavic et al. 2000).

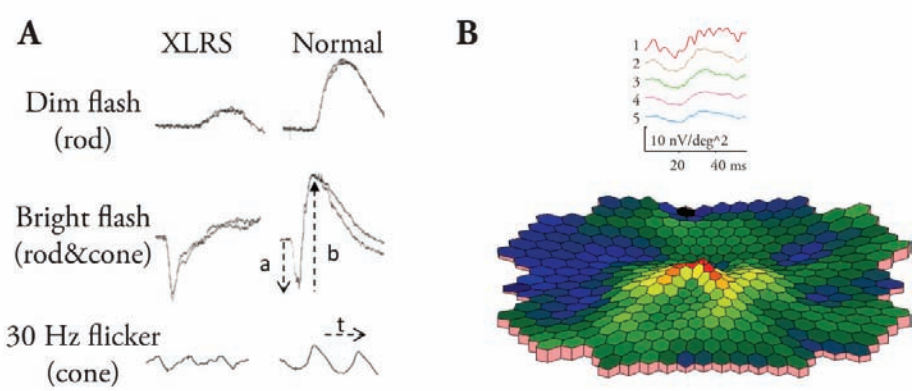

Figure 4. Typical electrophysiological findings in patients with X-linked retinoschisis. A.)Full-field ERG with reduced rod function in dim light, electronegative waveform with b-wave (b) smaller than a-wave (a) in bright flash ERG. Reduced amplitude and prolonged implicit time (t) in 30Hz flicker. B.) Multifocal Electroretinogram(mfERG) recording with reduced foveal amplitudes.

Treatment

Clinical care consists of careful observation of young males at risk on the basis of knowledge of the family pedigree. It is important that the young XLRS patients get a correct diagnosis because in many cases they benefit from low vision aid and educational support. Clinical observation continues throughout life, with particular attention to development of significant retinal inner leaf bullous separation and formation of outer retinal lamellar holes. Surgical repair of retinal detachment associated with X-linked retinoschisis is quite difficult and prone to failure.

Currently there are no proven treatments for XLRS. Various experimental treatment strategies have been considered, including the use of carbonic anhydrase inhibitors dorzolamide and acetazolamide (Apushkin and Fishman 2006; Ghajarnia and Gorin 2007), under the theory that the macular cystic spaces in human XLRS disease are filled with excess intraretinal fluid which impacts acuity. In one of the studies 7 out of 8 patients had an improvement in the degree of cystic foveal cavities in at least one eye evaluated with OCT, but functional improvement measured by visual acuity was modest (Apushkin and Fishman 2006). After withdrawal of the topical dorzolamide, the cavities reappeared, hence the treatment would most likely be life-long. A recent study noted that, in some cases, indirect manipulation of the retina through intraocular surgical vitrectomy causes collapse of the schisis cysts (Ikeda, Iida et al. 2008). None of these approaches are approved treatments for XLRS, nor is it known that any putative changes would persist beyond the acute intervention. Further, these approaches do not address the fundamental biological need for the retinoschisin protein in the retina nor the apparent role of this protein in synaptic integrity and function.

Aims of this study

General Aims

A translational investigation into whether supplementing the defective *RS1* gene with a functional *RS1* gene coding for the retinal structural protein retinoschisin using gene replacement therapy could restore visual function in patients with X-linked retinoschisis (XLRS).

Specific Aims

Paper I:

To create and evaluate a mouse model of human X-linked juvenile retinoschisis (XLRS) and investigate whether supplementing with the retinoschisin protein by gene delivery can reverse the abnormal "electro-negative" electroretinogram (ERG) retinal response and restore structural integrity of the retina.

Paper II:

To characterize the natural history of a retinoschisin gene knockout (*Rs1-KO*) mouse model and evaluate the long term effects of retinal rescue following AAV(2/2)-CMV-*Rs1* gene delivery.

Paper III:

To investigate the cellular consequences of retinal detachment in a retinoschisin gene knockout (*Rs1-KO*) mouse model.

Paper IV:

To evaluate long-term changes in retinal structure and function in patients with X-linked retinoschisis (XLRS) from childhood to adulthood.

Paper V:

To explore the influence of retinoschisin (RS1) protein, in human retinal detachment by analyzing vitreal RS1 protein levels in eyes with or without retinal detachment.

Subjects

Mice

A 17.5-kb mouse genomic DNA fragment was cloned from the mouse 129Sv/Ev λ genomic library, which contained exon 1 and most of intron 1 of the mouse *Rs1* orthologue of the human *RS1* gene. An 11-kb fragment cut by *Sma*I and *Not*I was used to make the targeting construct. All exon 1, including 9 bp upstream of the ATG start codon and a 1630-bp fragment of intron 1, was replaced by the neomycin resistance (*neoR*) gene cassette. Before electroporation, the targeting plasmid was linearized with *Not*I. The *Rs1*-knockout (*Rs1*-KO) was generated with assistance from Ingenious Targeting Laboratory, Inc. (Stony Brook, NY).
129Sv/Ev mouse embryonic stem cells were electroporated with linearized target plasmid DNA and selected using G418 antibiotic. DNA was isolated from neo-resistant colonies, and positive homologous recombination was identified by PCR analysis with the primer pair RSDA6 and PLA2. Primer RSDA6, located outside of the targeting construct, has a sequence of 5'-GGCAGTCCAGTCCCTGTAAGTGTG3'. Primer PLA2 is located in the 5 -promoter region of the *neoR* gene cassette and has a sequence of 5'-GTTCTTCGGACGCCTCGTCAACAC3'. The positive clones gave rise to a 2.4-kb PCR fragment.

A second primer pair, RS2 and RSWT1, gives a 550-bp PCR product that identifies the wild-type (WT) allele. Primer RS2 is located 530 bp upstream of the ATG start codon, with a sequence of 5'-CCTGATGACCTCTGGAATCTGCTC-3'. Primer RSWT1 is located 1 bp downstream of the ATG start codon and has a sequence of 5'-GAAGAAGCCTTCAATCTTGTGTGG-3'. A positive ES cell clone was expanded and microinjected into C57BL/6J blastocysts and eight chimeras with high-percentage coatcolor mottling were produced, of which four were

male. Three of these gave rise to germline transmission when bred to C57BL/6J females. Female F1 animals heterozygous for the *Rs1*-KO were crossed with WT C57BL/6J males to generate $Rs1^{-/Y}$ male offspring. These males were inbred to heterozygous females to produce homozygous female offspring.

Rs1-KO mice were genotyped by PCR methods using tail DNA as the PCR template, with two sets of oligonucleotide primers. One set was the primer pair RSDA6 and PLA2 that had been used to identify the targeted allele. An additional primer (5'-CCTTGTCCTTGGTCACAGCAAG-3'), located just before the ATG start codon, was designed to amplify the wild-type allele with primer RSDA6. Long-range PCR was performed in a 25 µl reaction containing 200 ng of tail DNA, 10 pMole of each primer, 2 mM $MgCl_2$, 400 µM deoxynucleotide triphosphates, 2 U of Taq DNA polymerase (Platinum; Invitrogen, Carlsbad, CA), and 2.5 µl of 10x reaction buffer supplied by the manufacturer. These conditions were used for amplification of both alleles: 3 minutes at 95°C for initial denaturation, followed by 40 cycles of 30 seconds at 95°C, 50 seconds at 66°C, 2 minutes 40 seconds at 72°C, and 10 minutes at 72°C, for the final extension. The annealing temperature was decreased 0.4°C per cycle after five cycles until it reached 62°C. The PCR products were 2.4 kb and were analyzed by agarose gel electrophoresis.

In paper II, *Rs1*-KO mice were studied ranging in age from 1-16 months, and age matched C57BL/6 wild type (wt) mice from Jackson Lab (Bar Harbor, Maine) were used as controls. Two months old *Rs1*-KO mice and wt littermate mice were used for immunocytochemical studies in paper III.

Patients

In paper IV, male patients from the Swedish RD-registry a national registry of patients with retinal degeneration in Sweden containing approximate 2800 patients, between 18 and 25 years of age with clinical diagnosed X-linked retinoschisis and with records of previous ophthalmologic examination, including full-field ERG at least eight years earlier, were included in this study. The clinical diagnosis of X-linked retinoschisis was based on the ocular history, funduscopic findings, visual fields, a modified ISCEV (International

Society for Clinical Electrophysiology of Vision) standard full-field ERGs and in some cases OCT when available. Based on these inclusion criteria, 20 eyes of 10 patients with XLRS (10 males; mean age 21.4 years; range, 18–25) were included in this study. The first examination was conducted between ages 6-15 years (mean age 9.3 years); mean interval between examinations was 12.1 years. All included patients were re-examined and underwent a complete ophthalmologic test including Snellen best corrected visual acuity (BCVA), full-field ERG, multifocal ERG, Goldmann visual field test, OCT and fundus photography. Blood was drawn for DNA analysis in 9 out of the 10 patients. Age matched controls for full-field ERG and mfERG responses were selected from a database of patients without signs of retinal degeneration using same standardized ERG protocols.

In paper V ten patients (average age 58 yrs) with primary retinal detachment of less than 7 days duration and with no previous retinal surgery were included. As normal controls, four patients (average age 70 yrs) with epiretinal membrane and with no previous retinal surgery were included.

Methods

Ethics

The animal studies were conducted in accordance with the National Institutes of Health (NIH) Animal Care and Use Committee protocols, the ARVO Statement for the Use of Animals in Ophthalmic and Vision Research, and the guidelines of the Animal Resource Center of the University of California Santa Barbara (Santa Barbara, CA).

The clinical study was conducted in accordance with the tenets of the Declaration of Helsinki and had the approval from the Ethics Committee, University of Lund. Informed consent was obtained from each of the patients after they were provided sufficient information on the procedures to be used.

Mouse *Rs1* cDNA Clone for Therapy Vector Construct

Rs1 cDNA was cloned from C57BL/6 mouse retina using RT-PCR methods. Mouse total retinal RNA was isolated, and single-stranded random hexamer-primed cDNA was generated by using Moloney murine leukemia virus reverse transcriptase (M-MLV RT; Invitrogen, Carlsbad, CA). A PCR primer set was designed to amplify the entire coding region of mouse *Rs1* cDNA (forward, 5'-GCCACCATGCCACACAAGATTGAAGGC-3'; reverse, 5'-CATCAGGCACACTTGCCGGC-3'). PCR was performed in a 50-µl reaction containing 2 µl of cDNA template, 12.5 pMole of each primer, 1.5 mM MgCl, 50 M deoxynucleotide triphosphates, 2.5 U Taq DNA polymerase (Platinum; Invitrogen), and 5 µl of 10x reaction buffer supplied by the manufacturer. The PCR amplification condition was 3 minutes of initial denaturation at 94°C, followed by 35 cycles of 30 seconds at 94°C, 30 seconds

at 58°C, 1 minute at 68°C, and 8 minutes of final extension at 68°C. The plasmid pCR-*Rs1* was generated by inserting the RT-PCR product into the pCR II-TOPO vector (Invitrogen), and the insert sequence was confirmed on a gene analysis system (CEQ 8000 Genetic Analysis System; Beckman, Fullerton, CA).

Generation of Recombinant AAV(2/2)-CMV-*Rs1* Vector

The Cis plasmid DNA of pAAV(2/2)-CMV-*Rs1*, in which the *Rs1* cDNA was driven by the CMV promoter, was made by inserting the 705-bp EcoRI fragment of the pCR-*Rs1* plasmid into the EcoRI restriction sites of the pZac2.1 vector provided by the Vector Core, Medical Genetics Division, Department of Medicine, Medical School, University of Pennsylvania. The recombinant AAV(2/2)-CMV-*Rs1* vector was generated using methods previously described (Auricchio, Kobinger et al. 2001; Hildinger, Auricchio et al. 2001). Briefly, HEK-293 cells were triple transfected with three plasmids at the Vector Core Facilities. The first plasmid encoded the *Rs1* expression cassette packaged between the AAV2 internal terminal repeats, the second encoded the rep and AAV2 cap genes, and the third encoded the adenoviral helper function genes. The AAV2/2-CMV-*Rs1* construct was purified by heparin column chromatography. The virus titer was assessed by real-time PCR, and the infectivity was assessed by an infectious center assay, as described previously (Salvetti, Oreve et al. 1998; Walz, Anisi et al. 1998). The ratio of the genomic copy number (GC) to the infectious center assay for this AAV(2/2)-CMV-*Rs1* construct was 39.

Delivery of Vector Construct to *Rs1*-KO Mouse Retina

Animals were anesthetized, and intraocular injections were performed with a technique similar to that described earlier (Bennett, Duan et al. 1997), by inserting a 33-gauge needle into the eye posterior to the limbus to deliver the vector-gene construct into the vitreous. In paper I *Rs1*-KO mice were given 2

µl AAV(2/2)-CMV-*Rs1* at a titer of 2.3×10^{10} GC/µl into the right eye. The contra-lateral left eye served as the control and either received 2 µl of phosphate-buffered saline (PBS) or remained untouched. In paper II seven *Rs1*-KO mice at post natal day 14(PND14) were given 1.5 µl of AAV(2/2)-CMV-*Rs1* at a titer of 2.3×10^{10} GC/µl into the right eye. The contra-lateral left eye served as the control and remained untouched.

Tissue Collection

Eyes from WT and *Rs1*-KO male mice were enucleated from freshly euthanized animals and fixed for histology either by transcardial perfusion with 2.0% paraformaldehyde (PFA) and 2.5% glutaraldehyde in 0.1 M cacodylate buffer, followed by overnight immersion in the same fixative, or by direct immersion for 24 hours in the fixative. In paper I, eyes for immunohistochemistry were immersed in 4% PFA/PBS overnight. PFA/PBS-fixed eyes were dehydrated in ethanol, cleared in xylene, and embedded in paraffin; PFA/PBS-fixed eyes used for confocal immunfluorescence microscopy were embedded in low melting temperature agarose (Sigma-Aldrich, St. Louis, MO) and sectioned. In paper II, perfusion fixed eye tissue was trimmed, post-fixed in 1% osmium tetraoxide/dH_2O for 1 hour and embedded in Araldite resin (Electron Microscopy Science, Hatfield, PA) for histological evaluation of the retina. In paper III, the eyes were first lightly cauterized to mark the hemisphere where the detachment originated (i.e., the region where the pipette tip penetrated the retina). The eyes were then enucleated and immersion fixed overnight in 4% paraformaldehyde in sodium cacodylate buffer (0.1 M; pH 7.4) at 4°C. The next day the cornea and lens were removed to form an eyecup, which was then bisected through the area of detachment. Sections were cut transversely through the bisected area of detachment. Briefly, the eyes were rinsed in phosphate-buffered saline (PBS; pH 7.4) three times for 15 minutes each and one time for 60 minutes, embedded in low-melt agarose (5%; Sigma-Aldrich, St. Louis, MO) at 45°C and subsequently sectioned at 100 m using a vibratome (Leica, Lumberton, NJ).

Antibodies and Immuno-histochemical Procedures

In paper I and II, a rabbit polyclonal RS antibody against the N-terminus of retinoschisin (amino acid residues 24-37, translated from *Rs1* exons 2 and 3) was used for immunofluorescence of mouse retinal specimens, as described previously (Takada, Fariss et al. 2004). Retinal sections cut at 8μm thickness were blocked in 10% normal goat serum in PBS and then incubated with RS antibody at 4°C overnight. After washing in phosphate buffered saline (PBS), sections were incubated with Alexa 568 goat anti rabbit IgG/DAPI (Invitrogen, Carlsbad, CA). Images were collected with Leica SP2 laser confocal microscope (TCS SP-2; Leica Microsystems, Exton, PA). Light microscopy was performed on paraffin-embedded, 4μm-thick, sections that were treated with 100 g/ L proteinase K at room temperature for 15 minutes for epitope unmasking. The avidin-biotinylated enzyme complex (ABC) method (Vector, Burlingame, CA) was used, and the antibody complexes were visualized with 3,3-diaminobenzidine (DAB).

In paper II,I immunocytochemistry was performed as described previously (Verardo, Lewis et al. 2008). To prevent nonspecific binding of antibodies, the reactions in the retinal sections were blocked overnight with normal donkey serum 1:20 in PBS containing 0.5% BSA, 0.1% Triton X-100, and 0.1% Azide (PBTA) at 4°C on a rotator for continuous agitation. After the overnight blocking step, the PBTA was removed and primary antibodies, diluted in PBTA, were added for another overnight incubation at 4°C. The next day retinal sections were rinsed in PBTA, three times for 15 minutes each and one time for 60 minutes, at which time the corresponding secondary antibodies were added for the last overnight incubation at 4°C. Antibodies to the following proteins were used: glial fibrillary acidic protein (GFAP) (1:400, rabbit polyclonal, DAKO, Carpinteria, CA), rod opsin (1:500, mouse monoclonal; a gift from Robert S. Molday, University of British Columbia, Vancouver), and neurofilament protein (1:500, mouse monoclonal; Biomeda, Hayward, CA). The secondary antibodies included donkey-anti mouse, goat, or rabbit conjugated to Cy2, Cy3, or Cy5 (Jackson ImmunoResearch, Laboratories, West Grove, PA). Finally, the sections were rinsed in PBTA as just described, mounted in 5% n-propyl gallate in glycerol on glass slides,

covered with a coverslip, and subsequently sealed with nail polish. In some cases, the sections were mounted in n-propyl gallate containing the nuclear stain Hoechst (1:5000; Molecular Probes, Eugene, OR). The specimens were viewed and images collected with a laser scanning confocal microscope (FluoView 500; Olympus Center Valley, PA). Rs1-KO, and control eyes from the same immunohistochemistry experiment were viewed during the same session, with black and gain levels kept constant to allow for comparisons and semi-quantitation of labeling intensity.

Histological Evaluation of the Mouse Retina

From eye cups embedded in Araldite resin, sections of 0.5 μm-thickness were cut along the vertical meridian passing through the optic nerve and stained with 0.1% toluidine blue for light microscopy. Photoreceptor cell loss with age was evaluated by counting ONL cells on photomicrographs of retinal sections taken with the 20x objective of a Nikon E800 photomicroscope and a DXM1200 digital camera. Inferior and superior retina were counted separately between 200 and 1200 um from the optic nerve (ON) using an automated method with ImageJ software (http://www.bioimage.ucsb.edu/software.html) with the ITNC nuclei detector plug-in (http://rsb.info.nih.gov/ij), as previously described (Byun, Verardo et al. 2006). The width of the photoreceptor outer segment layer (OSL) was measured perpendicularly between the retinal pigment epithelium (RPE) and the inner segment layer at 100 μm intervals in the same retinal regions. This measurement was used rather than the standard technique of measuring single rod outer segment (ROS) lengths because ROS in *Rs1*-KO mice were often disrupted and misaligned. The severity of retinal schisis cavities was assessed by five examiners who individually scored the size and extent of cavities on a scale of 0 to 4, zero indicating no cavities, using digital photomicrographs of retinal sections taken at 2x. This was done for both the inferior and superior halves of the retinal sections. The values for the size and the extent of cavities were multiplied together and normalized to a 0-100% scale with 0% being not affected. A similar technique has been used to assess photoreceptor survival in histological sections in light damage experiments.(LaVail, Yasumura et al. 1998) Measurements were done on 4 to 5 animals at each age.

Transient Experimental Retinal Detachment

In paper III, retinal detachments were produced in the right eyes of two month old *Rs1*-KO and C57BL/6J (wt) mice, and left eyes served as the control. First, a pilot hole was created with a 30-gauge needle through the sclera a few millimeters below the limbus. A fine custom-pulled glass micropipette was then introduced trans-vitreously and inserted between the neural retina and the RPE, at which time approximately 5 µl of balanced salt solution was infused, detaching approximately 75% of the retina. A glass cover slip, placed on the cornea, was used to visualize the retina during surgery. Since the glass pipette tip (1 cm long) was very thin and flexible, it did not penetrate or damage the lens; no cataracts were observed at the time of euthanatization. The mice were euthanatized at 1, 7, or 28 days after detachment. A 1-day animal is considered to have had a detached retina for the majority of the 24-hour period. As described in the Results section, since balanced salt solution was used to create the detachments, the retinas spontaneously reattached by 24 hours; hence, a 7-day animal is considered detached for 1 day and reattached for 6 days. Similarly, a 28 day detachment is considered having a 1-day retinal detachment followed by a reattachment period of 27 days.

Quantification of retinal changes after retinal detachment

The number of photoreceptor cells (i.e., number of nuclei/area of ONL) and schisis cavities, and the size of the schisis cavities relative to the area of the INL were all calculated from 50 to 100 randomly collected confocal images at a resolution of 512 by 512 with a pixel size of 0.62 m. These images were taken from the central to the mid-peripheral retina in each of the relevant animals (schisis cavities do not exist in wt mice). The number of photoreceptor nuclei was counted in the images with an automated computer program (Nucleus Detector, provided in the public domain at http://www.bioimage. ucsb.edu, Center for Bioinformatics, University of California at Santa Barbara) (Byun, Verardo et al. 2006). The area of the ONL within each image was also automatically calculated using the method previously described. An average

density of photoreceptors for all the animals within a group was then calculated using the average density per animal. To determine the number and area of the schisis cavities, borders were manually drawn around the cavities on the digital images (DiminViewer software; http://dimin.m6.net/software/viewer/ developed and provided in the public domain by Dimitry V. Federov under the auspices of several grantors). The average number of schisis cavities was calculated per millimeter of INL for each group of *Rs1*-KO animals. The area of the schisis cavities within an image was calculated by measuring the area of the cavities/the area of the INL 100 to give a percentage of INL area occupied by the cavities. These areas were averaged as described for photoreceptor cell counts to provide an overall average for each group. For statistical purposes, $P>0.05$ was not considered statistically significant

Determining a representative number for subretinal scars in the various samples was done somewhat differently in an attempt to avoid bias in selecting areas that have scars and yet assure that enough sampling area was obtained to allow for some measure of significance. In this case, central-to-peripheral retinal mosaics approximately 2 mm in length were constructed from one animal from the wt control, wt 7-day detached, *Rs1*-KO control, and *Rs1*-KO 7-day detached groups. There are no sub-retinal scars in the wt control animals. The data are presented as the number of scars per millimeter within the retinal mosaics.

Vitrectomy

All patients included in paper V underwent a standard 3-port PPV including a biopsy of 1-1.5 ml of undiluted central vitreous obtained under air infusion via suction through the vitrectomy probe (Innovit®, Alcon Laboratories, Forth Worth, Texas, USA). The sample was thereafter kept at -80 degrees C for later examination.

Western Blot Analysis

Wild-type mice and *Rs1*-KO mice were euthanatized by carbon dioxide, and retinas were dissected. The retinal extract was isolated with a mammalian cell lysis kit (Sigma-Aldrich) following the manufacturer's instructions. The protein concentration was determined with a bicinchoninic acid (BCA) protein assay reagent kit (Pierce, Rockford, IL). Thirty micrograms of protein from each sample were separated on duplicate 12% SDS PAGE gels, and one gel was transferred onto a nitrocellulose membrane for Western blot analysis; the duplicate gel was stained (Simply Blue SafeStain; Invitrogen) to demonstrate the equal loading of protein extract. After incubation with the same polyclonal RS1 antibody used for immunohistochemistry, RS1 was detected with a chemiluminescent Western blot detection reagent (ECL; Amersham Biosciences, Piscataway, NJ).

The vitreous samples, from patients in paper V, with equal amount of protein (20 µg protein) were electrophoresed on non-reducing 4-12% SDS-PAGE and immune-blotted with anti-RS1 antibody and identified using enhanced chemiluminiscence HRP functionalized substrates. The intensity of ~200 kDa RS1 band was analyzed on image station (Kodak 2000R). Relative intensity of each ~200kDa RS1 octamer band was calculated as a percentage of the intensity of the recombinant RS1 used as control.

Mouse Full-field Electroretinography

Full-field scotopic electroretinograms (ERG) were recorded from *Rs1*-KO and wild type C57BL/6 (WT) mice; recordings were obtained only once from each mouse. Mice were dark-adapted for 12 hours prior to anesthesia with intraperitoneal administration of ketamine (70-80 mg/kg) and xylazine (4-6 mg/kg), and the pupils were dilated with topical 0.5% tropicamide and 0.5% phenylephrine HCl. Mice were placed on a heating pad to maintain body temperature near 38°C. ERGs were recorded with gold wire loops placed on the cornea with a drop of methylcellulose after applying 1% proparacaine topical anesthetic; gold wire loops on the sclera at the limbus served as the

differential electrodes, and a ground wire was attached to the left ear. Scotopic ERG responses were elicited using single flashes from a Xenon discharge source (Grass Photic Stimulator PS33, Astro-Med Inc, West Warwick, RI) from -6.9 to +0.6 log cd•s/m^2 in 0.5 log steps or with bright photostrobe flashes (model 283; Vivitar, Santa Monica, CA) from +1.4 to +2.4 log cd•s/m^2. Stimuli were delivered in a Ganzfeld (full field) sphere with inter-stimulus intervals of 3 to 180 seconds, depending on stimulus intensity. A stimulus intensity range of -6.9 to +2.4 log cd•s/m^2 was obtained using neutral density filters (Wratten, Eastman Kodak, Rochester, NY). Photopic cone ERGs were elicited with 0.6 log cd•s/m^2 stimuli on a 42 cd•s/m white rod-suppressing background. Responses were amplified 5000 times and filtered using a 0.1 Hz and a 1 kHz high and low pass filter, respectively, and a 60 Hz line-frequency filter (CP511 AC amplifier, Grass Technologies, Astro-Med Inc, West Warwick, RI). A-waves were measured from the pre-stimulus baseline to the initial trough. B-waves were measured from the baseline or from the a-wave trough when present.

Human Full-field Electroretinography

Full-field ERG was recorded in a Nicolet analysis system (Nicolet Biomedical Instruments, Madison, WI, USA). After pupil dilation with topical cyclopentolate 1% and metaoxedrine 10% the subjects were dark adapted for 40 minutes and a Burian Allen bipolar contact lens was applied on the cornea and a ground electrode on the forehead. ERG recordings in young patients were performed under general anesthesia with propofol. Responses were obtained with a wide band filter (-3 dB at 1 Hz and 500 Hz) stimulating with brief (30 µs) single full-field flashes of dim blue light (Wratten filter #47, 47A and 47B) and white light (0.81 cd•s/m^2 and 3.93 cd•s/m^2). Cone responses were obtained with 30-Hz flickering white light (0.81 cd•s/m^2) averaged from 20 sweeps. If responses measuring less than 10 µV were recorded with single white flashes, recordings were also obtained with computer averaging (30 flashes), a bipolar artifact rejecter and a line frequency notch filter (50Hz). To obtain small cone responses, stimulation included 200 sweeps of 30-Hz flickering white light and a digital or analogue narrow band-pass filter added to the system.

Human Multifocal ERG

Multifocal electroretinography (mfERG) was recorded using the visual evoked response imaging system (VERIS 4; EDI, San Mateo, CA, USA) developed by Sutter et al(Sutter and Tran 1992; Bearse and Sutter 1996). The stimulus matrix consisted of 103 hexagonal elements displayed on a screen in the infrared (IR) camera. The recording procedures were performed according to the ISCEV guidelines for clinical mfERG (Hood, Bach et al. 2008). Recordings were monocular, and the fixation was controlled using the IR camera and infrared illumination from the recording electrode, with visualization of the hexagonal elements over the retina. The first order kernel P1 amplitudes and implicit times in ring areas 1 - 6 were calculated according to the guidelines for basic mfERG (Hood, Bach et al. 2008). Responses from ring areas 1 and 2 were averaged and noted as Ring (1+2).

Human Optical coherence tomography

In paper I, OCT was performed on both eyes using Zeiss Stratus OCT model 3000, a time domain ocular coherence tomography (OCT; Model 3000; Carl Zeiss Meditec, Dublin, CA). In paper IV, a spectral domain 3D OCT-1000 with version 3.00 software (Topcon, Tokyo) was used. 3D macula scan option was used for all scans in this study centered on the fovea covering 6 x 6 mm, resolution 512 x 128, imaging the complete macular area. The instrument utilizes a Fourier domain spectrometer producing cross-sectional B scans and 3-D volumetric images at a speed of 25,000 A scans /sec. OCT scans were used for classification of retinal phenotypes in XLRS using a modified version(Lesch, Szabo et al. 2008) of Prenner's "Classification scheme for XLRS(Prenner, Capone et al. 2006).

Human Mutation analysis

Blood samples were collected from all participants in paper IV after obtaining informed consent according to the Helsinki declaration. Genomic DNA was extracted from peripheral blood cells using QIAamp DNA Mini Kit, Qiagen GmbH, Hilden, Germany). RS1 gene coding regions (exons 1-6) and the

flanking intronic sequences were amplified by PCR with Platinum Taq DNA polymerase (Table 5 Paper IV) (Invitrogen, Carlsbad, CA, USA) in Peltier Thermal Cycler (BioRad Life Sciences, Hercules, CA, USA). The amplicons were analyzed on 1.4% agarose gels and stained with ethidium bromide and purified using QIAEX II gel extraction kit (Qiagen) according to the manufacturer's protocol. The purified amplicons were used as sequencing templates. Sequencing was carried out in ABI3730XL analyzer using Big Dye 3.1 sequencing kit (Applied Biosystems, Foster City, CA, USA). Sequences were assembled and analyzed with Lasergene SeqMan software. The results were compared with the RS1 reference sequence: ENSG00000102104 (http://uswest.ensembl.org/Homo_sapiens/Gene/Summary?db=core;g=ENSG00000102104). HGNC ID:10457

Statistics

Statistical analysis was performed on a computer (*SPSS statistical software*, ver. 17; *SPSS* Science, Inc., Chicago, IL). In paper II and III, Student's t-test was used to calculate for significant differences in retinal function. In paper IV Students' paired t-test was used to evaluate full field ERG and BCVA differences between the patient's eyes as well as differences between the same eyes over time. Mann-Whitney U, a non-parametric test for assessing whether two independent samples of observations come from the same distribution, was used to compare mfERG data.

Results

Paper I and II

Mouse model of X-linked retinoschisis

No naturally occurring animal model of X-linked retinoschisis is known to exist. Therefore, a transgenic knockout mouse model for the *Rs1*-gene (*Rs1*-KO), the murine orthologue of the human *RS1* gene involved in X-linked retinoschisis, was created by replacing exon 1 and 1.6 kb of intron 1 sequence in the *Rs1*-gene with a neomycin resistance expression cassette. This truncates transcription of the *Rs1* gene and eliminates expression of retinoschisin protein. Confirmation that retinoschisin protein production was blocked was seen by Western blot of total protein extract from the *Rs1*-KO mouse retina. Confocal immunohistochemistry using the polyclonal RS antibody on retinal sections (Fig 5) from wild-type mouse showed retinoschisin particularly at photoreceptor inner segments and also in the outer plexiform layer (OPL) and the inner nuclear layer (INL) (*left*). No RS expression was seen in the *Rs1*-KO mouse retina (*right*).

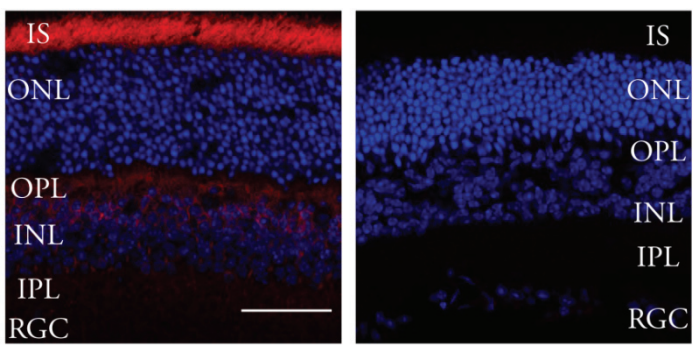

Figure 5. Confocal immunohistochemistry using polyclonal RS1 antibody on retinal sections. Retinoschisin was evident in WT mouse photoreceptor inner segments, the OPL, and the INL (left). No RS expression was detected in the retina of Rs1-KO mice (right). Scale bar, 50 μm.

Microscopy at 6 month of age showed that the *Rs1*-KO mouse retina had structural pathology equivalent to human X-linked juvenile retinoschisis (Fig. 6). Schisis dissection was seen through the inner nuclear layer (INL, *white arrows*) as structural gaps from intralamellar dissections, equivalent to "retinoschisis cavities." Schisis separations were also present in other retinal layers. The inner and outer plexiform layers, which contain the synaptic connections between photoreceptors and bipolar cells, were poorly formed and had irregular laminations. Some retinal ganglion cells (RGC) were mislocalized into the inner plexiform layer (*small dashed arrows*) and RGC duplication was observed (*large dashed arrow*). The photoreceptor layer was highly irregular, and some nuclei were mislocalized (*dashed circles*). Photoreceptor inner segments and outer segments (IS, OS) were short. The normal retina of a C57BL/6J littermate is shown at the left for comparison.

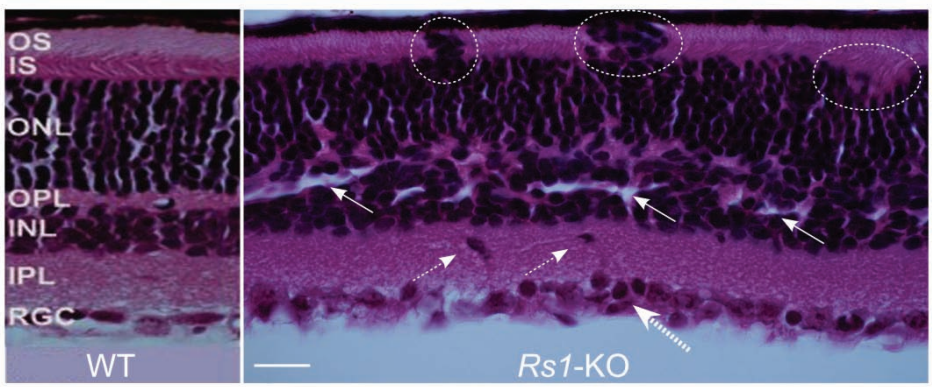

Figure 6. Retinal structure of *Rs1*-KO mouse. Retinal section exhibits many structural changes that include mislocalization (*small dashed arrows*) and duplication (*large dashed arrow*) of RGCs; dissection (*white arrows*) through the INL, poorly formed and irregular OPL, and irregular photoreceptor layer with photoreceptor nuclei mislocalized (*dashed circles*) into the shortened inner and outer segment layers (IS, OS). *Left*: normal C57BL/6J retina is shown for comparison. Scale bar, 50 µm. The mice were littermates, 6 weeks of age.

In paper II, we studied the natural retinal history of this retinoschisin knockout mouse out to 16 months of age. At 1 month, the outer nuclear layer (ONL) of *Rs1-KO* mice was disorganized but had nearly normal cell counts. The outer segment layer was thinned, rod outer segments were misaligned, and abundant schisis cavities spanned the inner nuclear and outer plexiform layers in all retinas. The *Rs1*-KO mouse exhibits a complex natural history of changes in retinal structure and function with age. Younger animals have more

accentuated schisis cavities than do older animals, with a peak time of cavities at approximately four months of age. In older age, the schisis cavities collapse and disappear. Concomitant with these cavity changes, the mice show a slow progressive loss of photoreceptor cells with age and by 16 month only about one-quarter of normal thickness was measured.

Retinal function

In paper I, we recorded the electroretinogram (ERG) to study the function of the retina in these newly created *Rs1*-KO mice, which confirmed a functional signaling abnormality (Fig. 7). Dark-adapted ERG amplitudes of *Rs1*-KO mice were approximately one-half that of wild type mice. The XLRS mouse ERG showed an "electronegative waveform" that is clinically pathognomonic of the human XLRS trait: positive-going b-wave amplitude (generated by the bipolar cells) is subnormal (*small arrows*), and at higher intensities the ERG has an "electronegative" waveform configuration (*bold arrows*) in which the b-wave amplitude is smaller than negative-going a-wave (generated by rod photoreceptors). An "electronegative ERG" is historically considered characteristic of human XLRS disease. This gives a reduced ratio of (b-wave/a-wave) that indicates a synaptic signaling deficiency between the photoreceptors and the second-order retinal bipolar neurons.

In paper II, we recorded the ERG in mice up to 16 months of age and found correlation with changes in retinal morphology. At 1 month, when a wildtype mouse retina is fully matured, the ERG a- and b- wave amplitudes were reduced by 33% and 50%, respectively, compared to wildtype. The a-wave reduction correlated well with the steady decline in ONL cell number. A rapid decline in the b-wave and a (b/a-wave) ratio less than in WT were associated with increasing severity of schisis cavities at young ages. At 4 months when the amount and size of cavities were at its maximum, the b/a-wave ratio was at its lowest point. The b/a-wave ratio was inversely correlated with cavity severity across all ages ($r=-0.74$, $p<0.0001$, $n=22$). Considerable heterogeneity was observed at each age in the ERG amplitudes and retinal morphology.

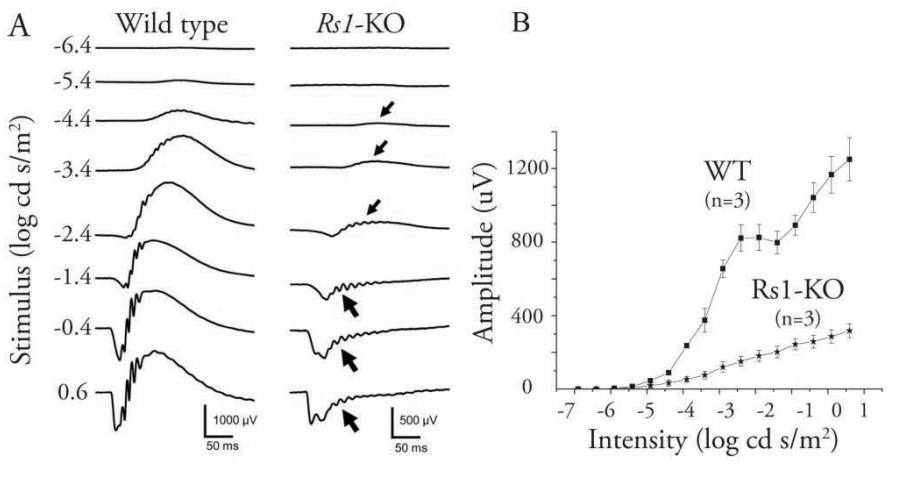

Figure 7. Retinal function of *Rs1-KO* mouse. A.)ERG dark-adapted intensity–response series from *Rs1-KO* mouse compared with WT shows subnormal amplitudes of positive-going b-wave (*small arrows*) resulting in an electronegative waveform configuration at higher intensities (*bold arrows*) with b-wave smaller than negative-going a-wave from rod photoreceptors. The mice were littermates and 6 weeks of age. B.) Amplitude versus log intensity (V-log I) curve of dark-adapted ERG recordings shows reduced b-wave response function for *Rs1-KO* compared with WT mice. Standard error bars are shown for three animals of each type.

Treatment with gene therapy

As described earlier in the Method section a recombinant AAV(2/2)-CMV-*Rs1* vector, i.e. an adeno-associated virus (AAV) serotype type 2/2, a cytomegalovirus (CMV) promoter and the Rs1 gene, was generated. Two micro-liters (2 µl) of the vector, at a titer of 2.3 E10 GC/µl, were injected in the right eye. The contra lateral left eyes served as the control and either received 2 µl of phosphate-buffered saline (PBS) or remained untouched. Injections were made in adult 13 week old mice, and ERG analysis and histology was done 9 -11 weeks later. After intraocular administration of the vector, immunohistochemistry showed retinoschisin expression in all retinal layers of *Rs1*-KO mice including an intense staining in the photoreceptors inner segment mimicking retinoschisin distribution in WT retina. The ERG recordings showed reversal of the electronegative waveform and restoration of the normal positive b-wave (Fig. 8).

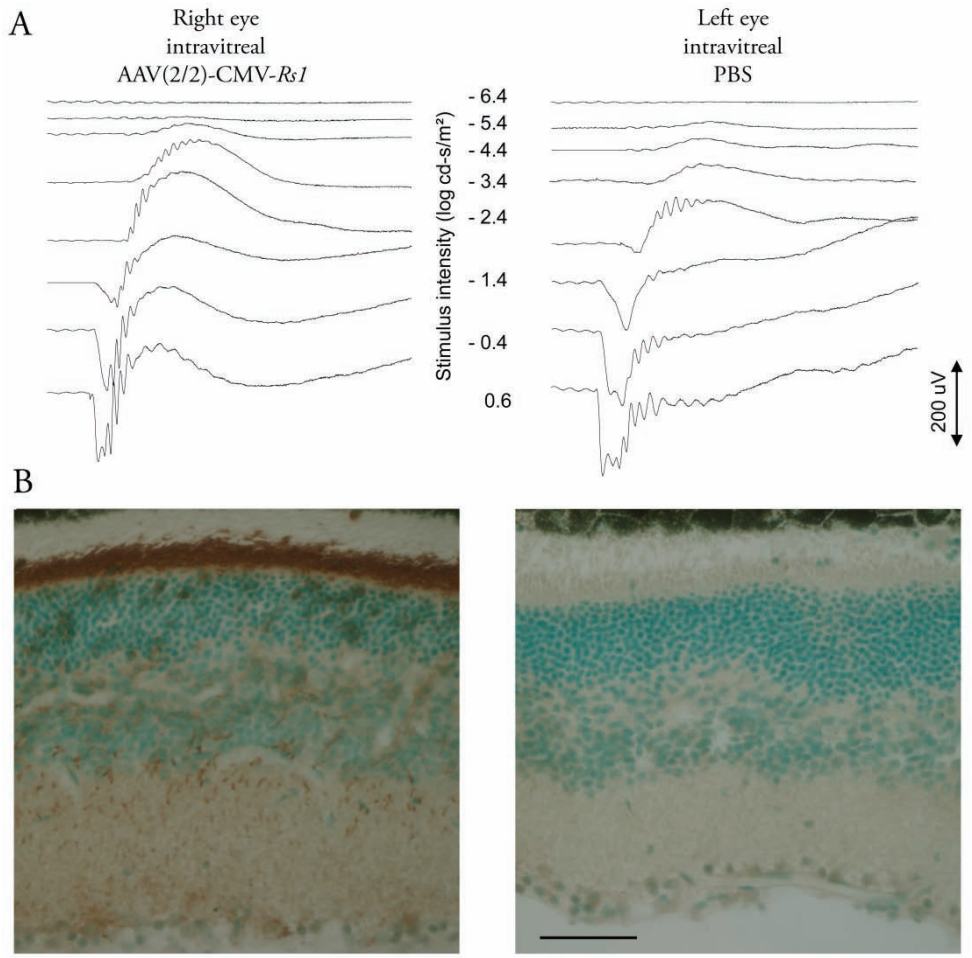

Figure 8. Effect on retinal function of adeno-associated virus AAV(2/2)-CMV-*Rs1* delivered by intraocular injection to the right eye of *Rs1*-KO mouse 554, with PBS injected into the left eye. Both eyes were injected at 13 weeks of age and were evaluated 9 to 11 weeks later (i.e., at 6 months of age). A.) ERG recording of control left eye (after PBS) shows the pathologic electronegative waveform characteristic of retinoschisis in the *Rs1*-KO. Right eye injected with AAV(2/2)-CMV-*Rs1* shows conversion of ERG waveform to the normal configuration characteristic of WT mice, with a typical positive-going b-wave greater than the negative a-wave. B.) Immunohistochemistry with a polyclonal RS antibody shows RS protein (*reddish brown* staining) in multiple retinal layers of right eye whereas no RS was evident in the PBS injected contra-lateral left eye. Scale bar, 50 µm.

We demonstrated in paper II long term rescue by Rs1 gene delivery to ameliorate the extent of progressive retinal changes in the Rs1-KO mouse retina. The mice were given intravitreal injection of AAV(2/2)-CMV-Rs1 vector in the right eyes at 14 days of age and then evaluated at the age of 14 months. The fellow eyes were untouched. Four out of seven mice showed a

substantially larger ERG in the treated eye than in the fellow control eye 14 months later. Results are shown below of retinal morphology and ERG from the animal with the greatest rescue (Fig 9). As described above, by 14 months *Rs1*-KO mice normally had severe reduction in the number of photoreceptor cells and few had persistence of well-formed inner and outer segments. As seen below, the ONL cell layer in the untreated eye was reduced 90% to about 1 cell thickness. The treated eye, however, had 4-5 rows of photoreceptor nuclei, and the RIS and ROS looked essentially like those of wild type but were 1/3 to 1/2 the length and, because of their structural preservation, were easily measured. The ERG b-wave intensity response relationship of the 14 month old treated eye was nearly identical to an average one month old *Rs1*-KO mouse. Immunohistochemistry (IHC) for retinoschisin protein was performed on one injected eye that showed rescue, and this eye was found to have strong expression of RS in the inner segment layer.

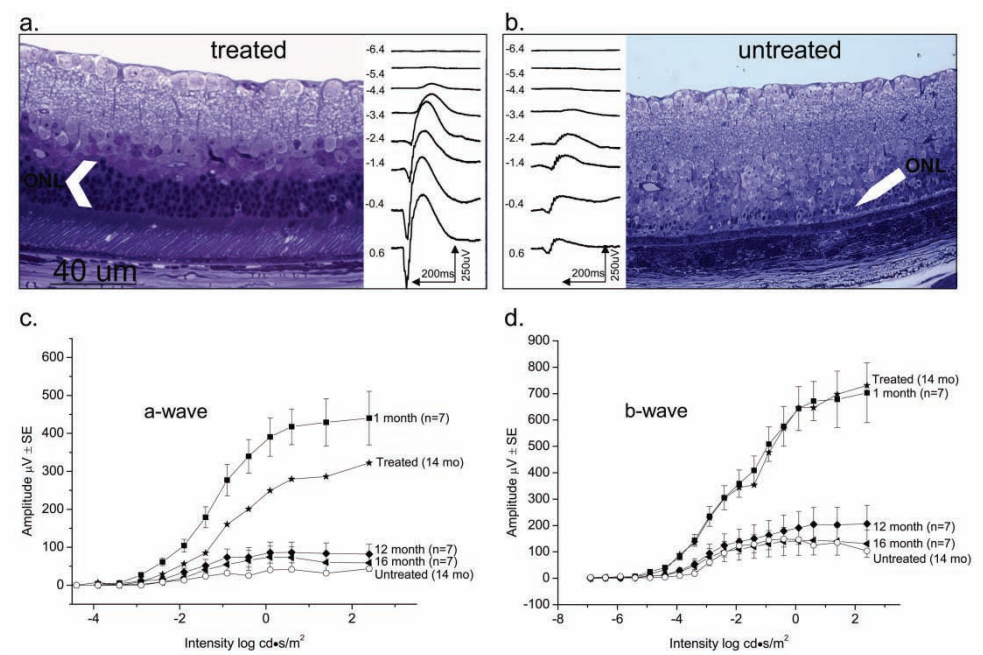

Figure 9. Long-term structural and functional rescue by AAV(2,2)-CMV*Rs1* in an *Rs1*-KO retina. Photomicrographs of sections of retinas from the treated (right) eye (**a**) and the untreated eye (**b**) 14 months after intravitreal gene delivery at 14 days of age. Half-micrometer sections were taken vertically through the optic nerve and stained with toluidine blue. V-log I curves of ERG a-wave (**c**) and b-wave (**d**) from treated and untreated eyes compared with average responses of different age groups.

We performed RS1 immunohistochemistry on the three eyes that failed to show rescue following AAV(2/2)-CMV-*Rs1* administration, and none showed expression of retinoschisin, leading us to conclude that the technique for gene delivery failed in these three attempts.

Paper III

Retinal Detachment

To investigate the cellular consequences of subretinal treatment delivery, that causes a temporary retinal detachment in patients with XLRS, we created large retinal detachments with balanced salt solution (BSS) in our retinoschisin gene knockout (*Rs1*-KO) mouse model. Since detachments were created with BSS, all retinas had spontaneously reattached by 1 day, both in wt and *Rs1*-KO mice.

Müller cells

In the *Rs1*-KO control eyes, there was a much greater expression of the intermediate filament protein GFAP than in the wt control eyes; anti-GFAP labeling of Müller cells extended from the ILM through the ONL in the *Rs1*-KO, whereas no Müller cell labeling was detected in the wt retinas. After detachment in wt animals at the 28-day time point anti-GFAP labeling had increased slightly in the Müller cells, but the labeling was still less than that observed in nondetached *Rs1*-KO eyes. No apparent difference in anti-GFAP labeling was observed between *Rs1*-KO detached and nondetached retinas at any time point. Anti-GFAP expressed by astrocytes also appeared similar in all animals and did not vary between wt and *Rs1*-KO or between attached and detached retinas. In our study, scars formed by Müller cells were observed in control *Rs1*-KO retinas, and they continued to be present after detachment, even though retinas had reattached by day 1. A hemi-section of an attached *Rs1*-KO retina shows several anti-GFAP-stained processes extending past the OLM where they disrupt the outer segment layer (Fig. 10). The prevalence of GFAP-positive processes crossing the OLM into the subretinal space was similar in the *Rs1*-KO detached (3.47/mm) and nondetached (3.40/mm) retinas and more than double the number than in wt detached retinas in the

same respective experimental group (1.5/mm), indicating that detachment did not increase the number of subretinal scars in the *Rs1*-KO retinas.

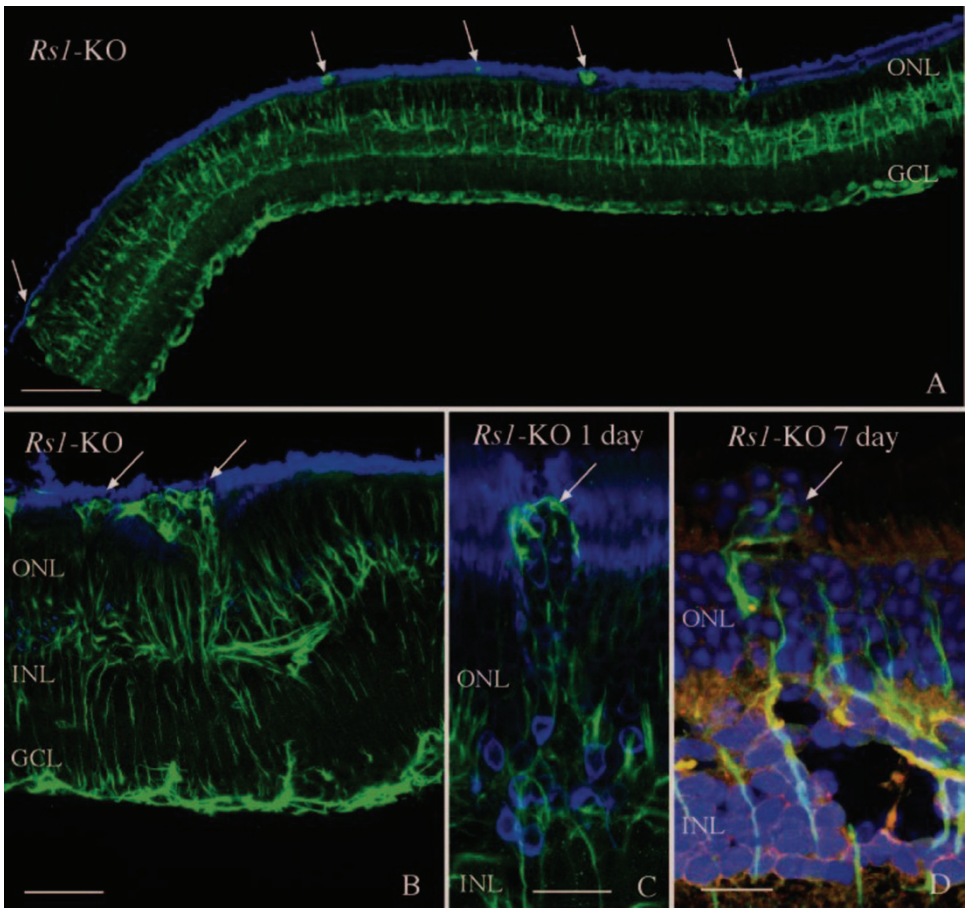

Figure 10. Laser scanning confocal images illustrating the presence of anti-GFAP labeled processes (*green*; *arrows*) in the subretinal space in nondetached (**A**, **B**) and detached (**C**, **D**) *Rs1*-KO retinas. Numerous anti-GFAP–labeled glial scars were observed in *Rs1*-KO retinas before detachment (**A**, **B**; *arrows*) resulting in photoreceptor outer segment disruption. A similar pattern of subretinal glial scars was observed after detachment (**C**, **D**; *arrows*). The presence of the scars was associated with a redistribution of the rod opsin protein (*blue*) to the ONL (**C**) as well as extrusion of photoreceptor nuclei (*blue*) into the subretinal space (**D**, *arrow*). Anti-rod opsin labeling is *blue* in (**A**), (**B**), and (**C**). Hoechst labeling of nuclei is *blue* in (**D**). GCL, ganglion cell layer.
Scale bars: (**A**) 100 μm; (**B**)50 μm; (**C**, **D**)20 μm

Schisis Cavities

The most prominent phenotypic feature of these *Rs1*-KO mice is the appearance of schisis cavities. Images from laser scanning confocal microscopy were used to quantitate the number of cavities/mm in detached and nondetached *Rs1*-KO. The number of cavities was significantly increased at day 1 of detachment but then decreased as the retina was reattached for longer periods of time so that their number did not show a statistically significant difference between the *Rs1*-KO control and the 7 or 28 day groups. However, there were significant differences in the area of the inner retina covered by the schisis cavities for the detached and nondetached *Rs1*-KO eyes. The area of the schisis cavities was consistently smaller overall in the detached *Rs1*-KO eyes when compared with the nondetached controls. The effect created a decrease in the average area of the INL occupied by schisis cavities from 17.48% in the *Rs1*-KO nondetached eyes to approximately 8.46% in the 28-day *Rs1*-KO animals.

Photoreceptor

Both nondetached and detached *Rs1*-KO retinas displayed focal regions of outer segment disruption and associated rod opsin redistribution adjacent to the subretinal scars. Photoreceptor cell bodies were present in the subretinal space within areas of the glial scars in both attached and detached *Rs1*-KO retinas. Rod opsin redistribution to the ONL was not observed in wt detached retinas, most likely because of the very brief period of detachment. To establish the magnitude of cell death occurring in the eyes, the density of photoreceptor cells (number of cells/mm2) was determined from retinal images using an automated cell counting program. Since we did not observe a decline in photoreceptor number in the left untouched control eyes of the *Rs1*-KO mice over the 1 month of this experiment, the ONL cell counts from those eyes were pooled to give an overall average of photoreceptor density in the *Rs1*-KO eyes. Cell counts from the left eyes of the wt control retinas were similarly pooled. The average cell densities were 51,764±3,483 cells/mm2 in wt animals and 49,976±3,027 cells/mm^2 in the *Rs1*-KO nonsurgical eyes. These data represent a difference of 3% and although small, show statistical significance when analyzed with a Student's t-test ($P<0.01$). The slight decline

in cell density in the wt mice in the 28-day experiment to an average of 50,844±1,952 cells/mm^2 does not show statistical significance. Although the decrease in photoreceptor cells in the *Rs1*-KO animals over the course of the study is small, the change between control 49,976 3,027 cells/mm^2 and 28 day animals 47,855 2,276 cells/mm^2 is statistically significant P<0.0001..

Neurite Outgrowth

It has been observed that retinas reacting to the loss of photo- receptor cells contain neurite processes that originate from both rod bipolar and horizontal cells, and most often grow into the ONL adjacent to a glial scar but sometimes into the inner retina as well. A recent study by Takada et al. also demonstrated neurite outgrowth from both rod bipolar and horizontal cells in *Rs1*-KO mice (Takada, Vijayasarathy et al. 2008). Positive neurofilament processes indicative of neurite outgrowth were observed extending into the inner and outer retina in all *Rs1*-KO mice. These processes were similar in appearance to those observed in wt mouse retina after 7 days of detachment, and they were morphologically consistent with processes arising from horizontal cells. Although the infrequency of these extensions made quantification difficult, our observations suggest strongly that there was no difference in the size or frequency of neurites in the *Rs1*-KO retinas whether detached or not. Double labeling experiments with anti-neurofilament and anti-GFAP suggest a clear morphologic association of neurites with reactive Müller cell processes growing past the OLM.

Paper IV

Ten patients with clinically diagnosed XLRS were included in the study and examined at two time points. The first examination was performed between ages 6-15 years (mean age 9.3 years) and all the patients were re-examined at the age of 18-25 years (mean age 21.4 years). The mean interval between examinations was 12.1 years.

Visual acuity

Best corrected visual acuity (BCVA) varied in this group of patients but demonstrated no significant change between a patient's right and left eye at

the measured time points (paired student's t-test p=0.64 ; p=0.116). Comparing BCVA between time points gave a small significance in the left eyes, with better BCVA at the later time point, but not in the right eyes (paired student's t-test p=0.305 ; p=0.048). At the first time point, patients between 6 and 15 years, demonstrated a positive correlation with age (Pearson Correlation 0.531 p=0.016) but at the later time point, the patients between 18 and 25 years did not show any correlation with age BCVA (Pearson Correlation -0.108 p=0.670).

Ophthalmologic examination

Fundus appearances, observed by indirect funduscopy, varied between patients, however, all patients had macular abnormalities at both first and second examination. The fundus findings demonstrated different degrees of retinal changes, including a spoke wheel pattern and a macular retinoschisis. Foveal retinoschisis was detected in 6 eyes of 3 patients by funduscopy and OCT, while macular lamellar schisis was visualized by OCT in 12 eyes of 6 patients. Structural and macular dysfunction was further examined with OCT and mfERG.

Visual field (VF) tests were assessed at both visits in seven of the patients, as three of them were too young to cooperate in visual field testing at the first visit. Repeated examination in seven of the patients demonstrated similar results compared with previous testing. Visual fields for outer borders tested with object V:4 was within normal limits in all these patients at both time-points, while inner borders tested with object I:4e demonstrated variable degrees of constriction in the visual fields of these patients.

Full-field ERG

A reduced rod b-wave amplitude, evaluated by full-field ERG blue light and white bright single flash, was demonstrated in all patients at both ages without any significant difference between the visits (Student's paired t-test bright flash b-wave OD p=0.142 OS p=0.573) or between eyes. Figure 11 shows the full-field ERG traces at 1st and 2nd visit from three representative cases. Cone amplitude and implicit time, measured by 30Hz flicker stimulation, showed a reduction in most of the patients but there was no significant difference between the two eyes or between visits (Student's paired t-test 30 Hz flicker amplitude OD p=0.981 OS p=0.683, 30 Hz implicit time OD p=0.904 OS p=0.325). A reduced b/a-wave ratio, reflecting a disruption between photoreceptors and second-order neurons, has been a hallmark of x-linked retinoschisis. In all examined patients this ratio was below normal, average 1.2±0.22 at first visit and 1.5±0.65 at follow-up visit compared with age matched normal 3.5±1.75 and 3.3±1.42.

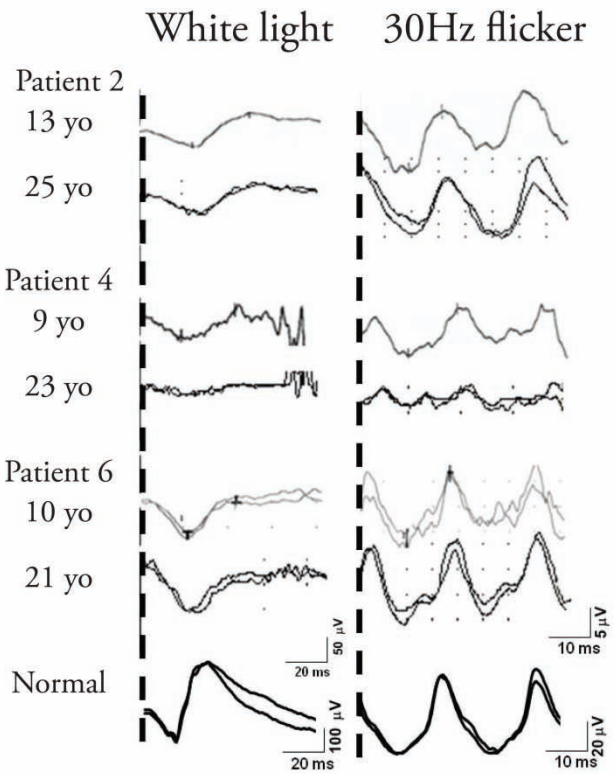

Figure 11 Full-field ERG traces at 1st and 2nd visit (3 cases). White light as a measurement of mixed rod cone function and 30 Hz flicker as a measurement of cone function. Note different scale for normal ERG traces.

Structure and retinal function in the macular region

Multifocal ERG and OCT

Multifocal ERG measured at the follow-up visit demonstrated localized reduced or subnormal cone function in the macular region in all patients and a significantly delayed implicit time in all rings. Optical coherence tomography revealed foveal schisis in various degrees and a thinning of the retina in some patients, while in some of the patients there were no schisis-like appearances in the macular or in the peripheral retina. The 3 patients that exhibited both lamellar and foveal schisis had the lowest central amplitudes.

Genetic analysis

PCR Amplification of the RS1 gene on individual genomic DNA samples covering the entire 6 exons with their flanking sequences was carried out in order to identify and confirm the mutations. Three different mutations were detected in these 9, patients including a known nonsense mutation in exon 3(Eksandh, Ponjavic et al. 2000). A novel one nucleotide insertion in exon 5 (c.421_422ins A; pArg141GlnX3) was identified in another patient. The 1-bp insertion of A residue at nucleotide 421 in exon 5 introduces an amber stop codon, UAG, that prematurely terminates translation—that is, a frame-shift change with Arg 141 as the first affected amino acid changing to Gln and creating a new reading frame ending in a UAG stop codon at position 3 (pArg141Gln fsX3). No mutations were detected in other patients examined although all coding regions and exon-intron boundaries were sequenced. It is possible that XLRS in these families is caused by a mutation located in the promoter or other regulatory regions, including those within introns or unknown splice variants that we didn't detect in this experimental setup. Interestingly, one such intronic mutation was observed in one patient, the atypical T>C transversion 35 bp downstream of 5' splice site of intron 3 (c.184+35T>C; g.IVS3+35T>C).

Paper V

RS1 protein

RS1 protein retinoschisin migrates as an octamer under non-reducing gels. Quantitative Western blot using anti-RS1 antibody on vitreous from patients with newly detached retinas showed a significant lower level of RS1 protein compared with vitreous from patients with non detached retinas (epiretinal membrane) (mean=0.3900 Range=0.39 n=10; mean=0.7695 Range=0.21 n=4; Mann Whitney U $p<0.01$).

Discussion

X-linked retinoschisis is a genetic retinal disease that affects 1:5000 to 1:25000 males worldwide and is one of the more common causes of vision loss from retinal degeneration affecting young men. Although Haas first described the clinical features of X-linked juvenile retinoschisis more than 100 years ago, it is actually not until recently that we have started to obtain a deeper knowledge of the pathophysiology involved in the disease. Earlier, it was frequently reported in ophthalmology textbooks that human XLRS was a stationary disease, but today it is believed to be progressive with age. Historically, this has been understated, presumably because the retinal changes progress more slowly than overt retinal degenerative diseases such as in typical retinitis pigmentosa. The human XLRS changes can typically be grouped into three age periods. Young affected males usually come to clinical attention on grade school vision screening exams. The condition then develops somewhat further over the grade school years into the teenage period, but is relatively stabilize throughout younger adult life. It progresses further in older adults who may develop macular atrophy and a further loss of central vision in older age. We reported in paper IV a clinical follow-up study of ten young XLRS patients, mean age 9 years at first visit, with typical congenital retinoschisis features. At follow up 12 years later, multifocal electroretinogram and ocular coherence tomography revealed a wide variety of structural and functional macular changes. Visual acuity assessment and electroretinogram revealed no significant decline in retinal function during this time period

In paper I, we generated a mouse model, Rs1-KO, deficient in Rs1 gene, to determine the role of RS1 protein, retinoschisin, in retinal structure and function. The hemizygous (Rs1-/Y) male mouse, as well as the homozygous female mouse (Rs1-/-), mimics structural features of human X-linked juvenile retinoschisis with progressive rod and cone degeneration, cystic dissection through, and disorganization of, multiple retinal layers. The Rs1-KO mouse

functional deficit results in an electronegative ERG waveform that is characteristic of human retinoschisis disease and that implicates a synaptic transmission deficit in the absence of retinoschisin protein. There is a large variability in retinal structure and function among same age litter mates, and the model exhibits a complex natural history of changes with age. Younger animals have more accentuated schisis cavities than do older animals; in older age, the schisis cavities collapse and disappear with time. Concomitant with these cavity changes, older Rs1-KO mice show a slowly progressive loss of photoreceptor cells and suffer a decline of function as observed by ERG recordings. This slow receptor cell death is also seen in the other XLRS mouse models (Min, Molday et al. 2005). Although essentially all photoreceptors are lost by 14-18 months of age in the Rs1-KO mouse retina, the natural history is unusual for the patchy distribution of photoreceptor loss. In this regard, the XLRS mouse model is atypical compared to the more uniform loss of photoreceptors in other rodent models of typical "retinitis pigmentosa," such as the rhodopsin transgenic mouse and rat, the RCS rat and the light damage rat. There are regional differences in the rate of photoreceptor death in some of these models rather than small patches of increased cell death.

Currently there are no proven treatments for this disease. Today, when more than 150 genes (http://www.sph.uth.tmc.edu/Retnet/ , May 2010) implicated in retinal diseases, including the *RS1* gene, are identified, a cure for XLRS is closer than ever. After the discovery of a blind Swedish Briard dog with a null mutation in RPE65 gene (Veske, Nilsson et al. 1998), the causative gene for Leber congenital amaurosis (LCA) in humans, treatment with adeno-associated virus (AAV) based gene replacement therapy has been demonstrated to improve retinal function in these dogs(Narfstrom, Katz et al. 2003; Weber, Rabinowitz et al. 2003; Acland, Aguirre et al. 2005; Le Meur, Stieger et al. 2007). The general strategy and efficacy of ocular gene transfer as means to deliver essential proteins to the retina to treat genetic recessive disease has recently been validated for the application of AAV vector-based ocular gene therapies in the clinic as well. Three separate groups evaluated the clinical use of AAV vectors for the treatment of LCA (Bainbridge, Smith et al. 2008; Cideciyan, Aleman et al. 2008; Maguire, Simonelli et al. 2008). The preliminary reports indicate that AAV vectors expressing RPE65 were administered by subretinal injection, and the majority of the treated subjects

showed evidence of improvement in retinal function, visual acuity, or reduction in nystagmus despite their relatively advanced state of retinal degeneration. Importantly, no vector-related adverse events were reported.

Sparing of heterozygous female X-linked retinoschisis carriers is likely due to the nature of the product of the *RS1* gene product, the retinoschisin protein. Evidence indicates that retinoschisin is a secreted protein, and even a reduced amount of protein synthesized in the retina of a female carrier appears to fulfill its function as a putative adhesion/stabilization molecule. As a consequence of random inactivation of one X chromosome on a cellular level in female cells, i.e. lyonization, the retinas of XLRS carrier women will contain a mixture of both normal and mutant gene products, and the lack of overt retinopathy in carriers thereby argues against a dominant negative effect of mutant retinoschisin protein. If a dominant negative effect existed for XLRS, the mutant gene product would interact with normal retinoschisin, preventing its function and thus resulting in an XLRS phenotype in the heterozygous carrier women. This observation is relevant for an attempt to deliver a normal *RS1* gene to an affected male, since it implies that the mutant gene and gene product are unlikely to interfere with the function of normal retinoschisin protein upon delivery of a normal *RS1* gene copy. The absence of clinical disease in carrier women also implies that the replacement level of expression need not reach that found in normal retinas to promote substantial, therapeutic function. These encouraging results provide the foundation for the development of AAV vector-based therapeutics for the treatment of XLRS.

To explore the viable use of gene replacement therapy as treatment for XLRS, we delivered an AAV serotype 2 vector containing the mouse *Rs1* cDNA under the control of CMV promoter (AAV(2/2)-CMV-*Rs1*) into the vitreous space of the right eyes of our *Rs1*-KO mice. The left eyes were either injected with saline or not touched and served as controls. In paper I, we injected into adult mice and ERG recordings and immunocytochemical studies were carried out to determine the effect of gene delivery on the recovery of retinal structure and function. These showed, a few months after delivery, staining of retinoschisin in all retinal layers of *Rs1*-KO mice including an intense staining in the photoreceptors inner segment mimicking retinoschisin distribution in WT retina. The ERG recordings showed reversal of the electronegative waveform

and restoration of the normal positive b-wave. In paper II, we treated the mice at an earlier time point, 14 days, and followed them out to 14 months. We demonstrated both structural and functional long term rescue in the *Rs1*-KO mouse retina. This signifies that gene replacement therapy through intravitreal delivery is a feasible strategy of therapeutic intervention both early and in the post-developmental adult stage of XLRS disease.

Min et al. (2005) reported that AAV5-mediated delivery of *Rs1* gene by subretinal injection transduced photoreceptor cells of *Rs1*-KO mice resulted in recovery of retinal structure and function over the long term. Due to the loss of retinoschisin which functions as a stabilizing retinal protein, subretinal injection in human retinas with schisis pathology may be technically challenging and pose a significant risk to the existing visual function of the subject. Vitrectomy is usually performed prior to subretinal injection. Adhesion of the vitreous to the retina may cause further laminar splitting of the fragile XLRS retina when the surgeon attempts to separate the vitreous from the retina. Additionally, the injection in the subretinal space may itself also pose difficulties. The tip of the injection needle must be positioned deep enough that the vector solution is not inadvertently routed into schisis cavities and thereby exacerbate the intraretinal splitting. In paper III, we studied the effect of transient subretinal detachments and conclude that large short-term detachments in *Rs1*-KO mice, followed by a period of reattachment may cause a slight increase in photoreceptor cell death, but detachments do not accentuate the gliosis and neurite sprouting. These findings suggest that performing subretinal injections to deliver therapeutic agents may be a viable option in the treatment of patients with retinoschisis without causing significant cellular damage to the retina. This delivery strategy may be problematic for an XLRS trial for other reasons. For example subretinal injection gives geographically localized delivery (Cideciyan, Aleman et al. 2008), while retinoschisin protein is expressed throughout the retina. Thus, optimal treatment of the disease would best be done by transduction of the entire retina. Vector delivery by subretinal injection is limited maximally to approximately 25% of the retinal area. While this amount of transduction is sufficient to cover the vicinity of the macula, much of the retina would probably not be transduced, and the untreated area would remain susceptible to retinal detachment and vitreous hemorrhage, which are a major cause of

vision loss in this disease. Some additional spread of retinoschisin has been reported in retinas of mice transduced by subretinal injection (Min, Molday et al. 2005), but it is not clear how this might scale to human subjects.

In patients with x-linked retinoschisis the retina is more prone to retinal detachment compared to the general population (10 vs. 0.01%, respectively) (Kellner, Brummer et al. 1990; Sasaki, Ideta et al. 1995). These detachments are usually difficult to surgically reattach, making the postoperative outcome unfavorable (Regillo, Tasman et al. 1993; Rosenfeld, Flynn et al. 1998). The RS1-protein mRNA level has recently been reported to increase during induced retinal detachment in mice (Farjo, Peterson et al. 2008). If the RS1 protein has a role in re-modeling the retina after a retinal detachment, this could be of major potential for future treatment of detachment in XLRS patients as well as in non XLRS patients with primary retinal detachment. To explore the influence of RS1-protein in human retinal detachment, we compared, in paper V, vitreal RS1 protein levels in eyes with or without detachment and found altered levels. The role of RS1 protein in the healing (re-modeling) process after retinal detachment is still unknown, and further investigation is needed. This finding demonstrates a possible role of RS1 protein in retinal detachment and may be of interest in the choice of surgical technique for the treatment of retinal detachment.

Conclusions

X-linked retinoschisis is a congenital progressive inherited retinal disease that affects the entire retina. The progression is variable but seems to be relatively stationary in the ages 6 to 25 years. Patients with XLRS lack a functional retinoschisin protein in the eye, because of mutation in the *RS1* gene.

Retinoschisin may play a role in reattachment of the retina after detachment

Electroretinography is an important tool for examining retinal function in these patients.

Our transgenic knockout mouse with a null mutation in the *Rs1*-gene is a valid model for human XLRS. It exhibits both structural and functional retinal changes similar to the human disease.

Intravitreal gene replacement therapy with an adeno-associated virus vector containing a functional *Rs1* gene showed structural and functional rescue in this XLRS mouse model both long and short term.

Populärvetenskaplig sammanfattning

Ärftliga näthinnesjukdomar är den vanligaste orsaken till grav synskada hos unga människor i västvärlden och X-bunden retinoschis (XLRS) är en av dessa sjukdomar som drabbar ungefär en på 5000 - 25000 personer. Näthinnan, retina, som är en specialiserad vävnad som utkläder ögats insida baktill innehåller celler som är känsliga för ljus, fotoreceptorer, kallade tappar och stavar. I fotoreceptorerna finns ämnen som vid ljuspåverkan startar en kedjereaktion i cellen, vilken resulterar i att ljuset omvandlas till en elektrisk signal. De nervsignaler som skapas genomgår sedan en komplex behandling av näthinnas övriga nervceller. Signalen skickas sedan, via synnerven och synbanan, in till syncentrum i bakre delen av hjärnan. Näthinnan innehåller omkring 130 miljoner fotoreceptorer (Fig. 12).

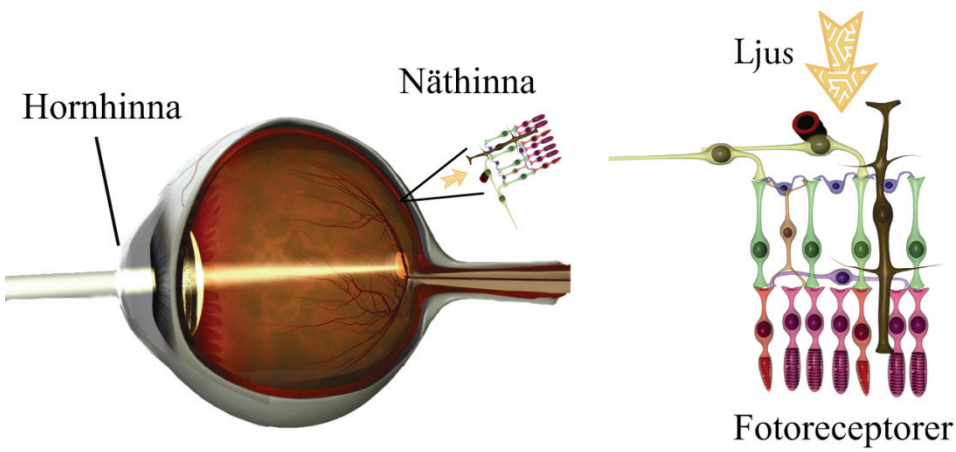

Figur 12. En förstoring av näthinnan som är en specialiserad vävnad som utkläder ögats insida baktill och innehåller celler som är känsliga för ljus, fotoreceptorer, kallade tappar och stavar. (Courtesy of Dr Fredrik Ghosh, Dep. of Ophthalmology, Lund, reproduced and modified with permission)

X-bunden retinoschis förekommer nästan uteslutande hos män och orsakas av en X-bunden genetisk defekt, som påverkar synen hos män som ärvt sjukdomen från sina mödrar som är opåverkade bärare. Ordet ”schis” kommer från det grekiska ordet för delning, som beskriver uppdelningen av näthinnans lager från varandra. XLRS diagnostiseras vanligen i samband med 4-års kontroll eller i början på skolgången pga. dålig syn och svårigheter med läsning. I svårare fall kan ofrivilliga ögonrörelser (nystagmus) ses redan i spädbarnsåldern. Synskärpan förblir väsentligen oförändrad hos de flesta mellan tonåren och fyrtio- femtioårsåldern, när en successiv försämring av näthinnan i gula fläcken brukar uppstå. Sällsynta fall förekommer där allvarliga komplikationer utvecklas, såsom separation av näthinnans lager (näthinneavlossning) eller läckage av blodkärl i näthinnan (glaskroppsblödning). Dessa ögonkomplikationer kan orsaka ytterligare nedsatt syn eller blindhet. En del i utredningen för att faställa sjukdomen är att använda elektrofysiologiska metoder (Electroretinogram, ERG), vilka objektivt mäter näthinnans funktion. En annan mycket viktig del i utredning är analys av patientens arvsmassa. På senare år har man hittat mer är 150 gener som är delaktiga i ärftliga ögonsjukdomar.

Gener, som transporteras på kromosomer är de grundläggande fysiska och funktionella enheter av arvsmassan. Det finns 46 kromosomer i nästan varje cell i människokroppen. De 46 kromosomer är arrangerade i par, 22 st. som kallas autosoma kromosomer och 1 par som är könskromosomer. Vi ärver en kromosom i varje par från vår mor och en från vår far. Könskromosomerna avgöra huruvida en person är kvinna eller man. Om det finns två X-kromosomer blir det en kvinna och om en X och en Y finns blir det en man. Gener är särskilda sekvenser av baser som kodar för instruktioner om hur man gör proteiner (äggviteämnen). Även om gener får mycket uppmärksamhet så är det proteinerna som utför de flesta livsnödvändiga funktioner och även utgör majoriteten av cellulära strukturer (Fig. 13). När gener ändras så att det kodade proteinerna inte kan utföra sina normala funktioner, kan genetiska sjukdomar uppkomma. I de flesta studier involverande genterapi så infogas en "normal" funktionsduglig gen i genomet för att ersätta den "skadade" sjukdomsframkallande genen. En transportörmolekyl som kallas ”vektor” kan användas för att leverera den terapeutiska genen till patientens celler. För närvarande är den vanligaste vektorn ett virus som är genetiskt förändrat.

Virus har utvecklat ett sätt att kapsla in och leverera sina gener till mänskliga celler och detta är ofta sjukdomsframkallande hos människan. Forskare har försökt att utnyttja denna förmåga och manipulera virusgenomet genom att ta bort de sjukdomsframkallande generna och ersätta med terapeutiska gener. Målcellerna, t ex näthinnans celler infekteras med den konstruerade virusvektorn som i sin tur kopierar det genetiska materialet, innehållande den terapeutiska mänskliga genen, in i cellen. På så får man cellen att producera ett nytt funktionellt protein och förhoppningsvis leder detta till att man botar sjukdomen

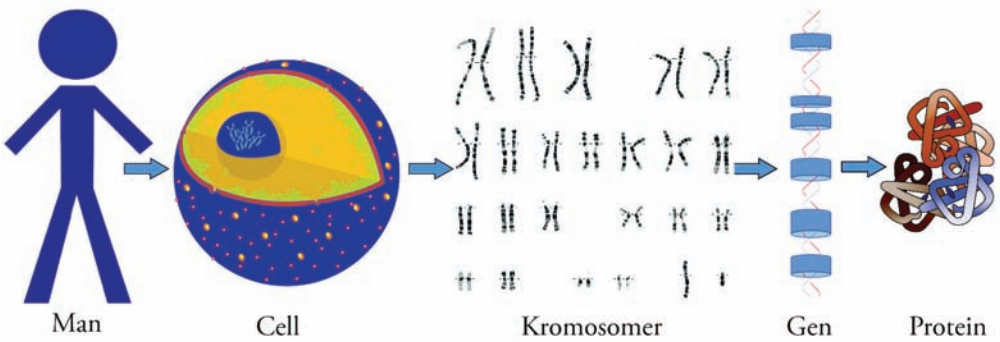

Figur 13. Människans arvsmassa ligger kodade på kromosomer i kroppens alla celler. Gener är särskilda sekvenser av baser som kodar för instruktioner om hur man gör proteiner som in tur utför de flesta livsfunktioner och även utgör majoriteten av cellulära

I denna avhandling har vi följt patienter med ögonsjukdom XLRS där man har hittat fel i en av könskromosomerna, x-kromosomen. Då kvinnor har två x-kromosomer blir de oftast endast bärare av sjukdomen och har normal syn. Män, som endast har en x-kromosom, får antingen sjukdomen ärvd från modern eller blir helt frisk från denna sjukdom. En man kan ej ärva XLRS från sin far men en dotter blir alltid bärare om pappan har sjukdomen.

För att studera sjukdomen x-bunden retinoschis närmare och för att kunna se effekten av genterapi skapade vi en musmodel av denna sjukdom, dvs. en genetiskt modifierad mus med fel i samma gen, retinoschisin-genen *Rs1*, som patienter med XLRS har. Denna musmodel visade sig vara en bra modell för

sjukdomen med jämförbara förändringar i näthinnans struktur och funktion. Vi gick vidare på ovanstående vis med att skapa en virusvektor som innehöll den friska *Rs1*-genen och injicerade denna i ögat på vår musmodel (Fig. 14). Både på kortsikt, efter några månader, och på långsikt, upp till 14 månader, såg vi en förbättrad näthinnestruktur och framförallt så kunde vi med ERG verifiera att funktionen på näthinnan var klart förbättrad.

Detta ger oss hopp om att i en snar framtid med genterapi kunna behandla patienter med X-bunden retinoschsis.

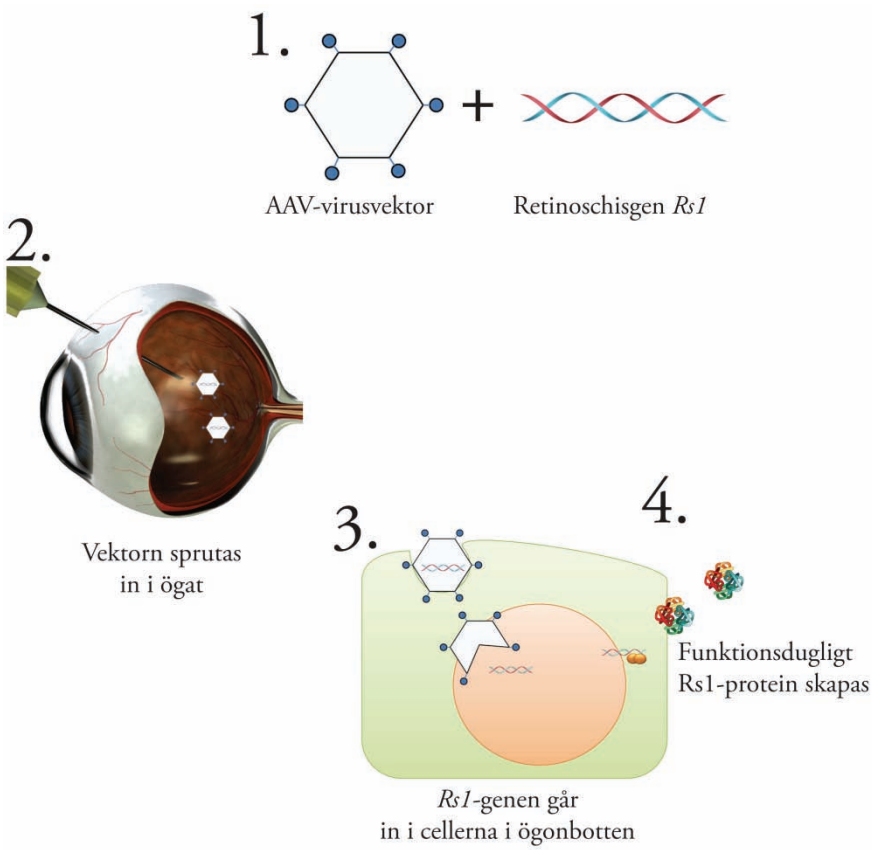

Figur 14. Genterapi med retinoschisgen. **1**.) En fungerande *Rs1*-gen kopplas ihop med en virusvektor. **2**.) Virusvektorn sprutas in I glaskroppsrummet i ögat. **3**.) Den fungerande *Rs1*-genen levereras till cellkärnorna i ögonbotten. **4**.) Cellen kan med den nya *Rs1*-genen skapa funktionsdugligt Rs1-protein.

Acknowledgements

Many people have been of invaluable assistance in the completion of this thesis, both professionally and personally. I would especially like to acknowledge and express my heartfelt gratitude to the following:

My supervisor and mentor, Sten Andréasson, for introducing me to the field of electrophysiology and always vital encouragement and support.

My supervisor, Vesna Ponjavic, for her unflagging enthusiasm and scientific support.

Paul Sieving, who gave me the opportunity to work with him in the NIH lab and guided me through years of scientific research there, for his encouragement and reminders that science is fun.

Ronald A. Bush, for his excellent mentorship and numerous discussions.

Yong Zeng, for many interesting discussions, both scientific and personal, and for teaching me about the wonderful world of genes.

Vijayasarathy Camasamudram, for his never-failing support and enthusiasm.

Maria Santos, for keeping track of me in the lab and always being a friend.

Jinbo Lee, for excellent technical work and all the lucky numbers.

Atsuhiro Tanikawa, for introducing me to the field of electrophysiology in our small friends.

Yuichiro Takada, for excellent technical work.

Dorit Raz-Prag, for many interesting scientific and cultural discussions.

Lucia Ziccardi, for continuing the good work in the lab.

Fredrik Ghosh, for help with designing the cover.

Steve Fisher, Geoff Lewis, Mark Verardo, Gabriel Luna and all the other members of Steve's lab in Santa Barbara UCSB, for great collaboration.

Boel Nilsson and Ing-Marie Holst, for skillful technical assistance.

Charlotte Hvarfner, for being my clinical mentor and friend.

The entire Association of Smart Scientists at NIH, for always having interesting topics to discuss.

Rikard, Emil and Julia Linnér, for always being there.

Aymeric Rivollier, JTADPEPCJ

Colleagues and friends at the clinic in Lund, all my friends in Sweden and the US, and finally my family, for everything.

References

Acland, G. M., G. D. Aguirre, et al. (2005). "Long-term restoration of rod and cone vision by single dose rAAV-mediated gene transfer to the retina in a canine model of childhood blindness." Mol Ther **12**(6): 1072-82.

Apushkin, M. A. and G. A. Fishman (2006). "Use of dorzolamide for patients with X-linked retinoschisis." Retina **26**(7): 741-5.

Auricchio, A., G. Kobinger, et al. (2001). "Exchange of surface proteins impacts on viral vector cellular specificity and transduction characteristics: the retina as a model." Hum Mol Genet **10**(26): 3075-81.

Bainbridge, J. W., A. J. Smith, et al. (2008). "Effect of gene therapy on visual function in Leber's congenital amaurosis." N Engl J Med **358**(21): 2231-9.

Bearse, J. M. A. and E. E. Sutter (1996). "Imaging localized retinal dysfunction with the multifocal electroretinogram." Journal of the Optical Society of America A **13**(3): 634-640.

Bennett, J., D. Duan, et al. (1997). "Real-time, noninvasive in vivo assessment of adeno-associated virus-mediated retinal transduction." Investigative ophthalmology & visual science **38**(13): 2857.

Bradshaw, K., N. George, et al. (1999). "Mutations of the XLRS1 gene cause abnormalities of photoreceptor as well as inner retinal responses of the ERG." Doc Ophthalmol **98**(2): 153-73.

Breton, M. E., A. W. Schueller, et al. (1994). "Analysis of ERG a-wave amplification and kinetics in terms of the G-protein cascade of phototransduction." Invest Ophthalmol Vis Sci **35**(1): 295-309.

Byun, J., M. R. Verardo, et al. (2006). "Automated tool for the detection of cell nuclei in digital microscopic images: application to retinal images." Mol Vis **12**: 949-60.

Cideciyan, A. V., T. S. Aleman, et al. (2008). "Human gene therapy for RPE65 isomerase deficiency activates the retinoid cycle of vision but with slow rod kinetics." Proc Natl Acad Sci U S A **105**(39): 15112-7.

de Jong, P. T., E. Zrenner, et al. (1991). "Mizuo phenomenon in X-linked retinoschisis. Pathogenesis of the Mizuo phenomenon." Arch Ophthalmol **109**(8): 1104-8.

de la Chapelle, A., P. Harper, et al. (1994). "A European research conference on the inherited disorders and their genes in different European populations." Eur J Hum Genet **2**(3): 191-2.

Deutman, A. F. (1971). The hereditary dystrophies of the posterior pole of the eye. Assen,, Van Gorcum.
Dewar, J. (1877). "The physiological action of light." Nature **15**: 433-435.
Eksandh, L. C., V. Ponjavic, et al. (2000). "Phenotypic expression of juvenile X-linked retinoschisis in Swedish families with different mutations in the XLRS1 gene." Arch Ophthalmol **118**(8): 1098-104.
Farjo, R., W. M. Peterson, et al. (2008). "Expression profiling after retinal detachment and reattachment: a possible role for aquaporin-0." Invest Ophthalmol Vis Sci **49**(2): 511-21.
Forsius, H., U. Krause, et al. (1973). "Visual acuity in 183 cases of X-chromosomal retinoschisis." Can J Ophthalmol **8**(3): 385-93.
George, N. D., J. R. Yates, et al. (1995). "Infantile presentation of X linked retinoschisis." Br J Ophthalmol **79**(7): 653-7.
George, N. D., J. R. Yates, et al. (1995). "X linked retinoschisis." The British journal of ophthalmology **79**(7): 697-702.
Gerth, C., R. J. Zawadzki, et al. (2008). "Retinal morphological changes of patients with X-linked retinoschisis evaluated by Fourier-domain optical coherence tomography." Arch Ophthalmol **126**(6): 807-11.
Ghajarnia, M. and M. B. Gorin (2007). "Acetazolamide in the treatment of X-linked retinoschisis maculopathy." Archives of ophthalmology **125**(4): 571.
Granit, R. (1933). "The components of the retinal action potential in mammals and their relation to the discharge in the optic nerve." The Journal of Physiology **77**(3): 207.
Haas, J. (1898). "Ueber das Zusammenvorkommen von Veranderungen der Retina und Choroidea. ." Arch Augenheilkd **37**: 343-8.
Hildinger, M., A. Auricchio, et al. (2001). "Hybrid vectors based on adeno-associated virus serotypes 2 and 5 for muscle-directed gene transfer." J Virol **75**(13): 6199-203.
Hiriyanna, K. T., E. L. Bingham, et al. (1999). "Novel mutations in XLRS1 causing retinoschisis, including first evidence of putative leader sequence change." Human mutation **14**(5): 423-427.
Holmgren, F. (1865). "Metod att objectivera effecten af ljusintryck på retina." Upsala Läkaref Förh **1**: 184-198.
Hood, D. C., M. Bach, et al. (2008). "ISCEV guidelines for clinical multifocal electroretinography (2007 edition)." Documenta Ophthalmologica **116**(1): 1-11.
Hotta, Y., M. Nakamura, et al. (2001). "Different mutation of the XLRS1 gene causes juvenile retinoschisis with retinal white flecks." Br J Ophthalmol **85**(2): 238-9.
Ikeda, F., T. Iida, et al. (2008). "Resolution of retinoschisis after vitreous surgery in X-linked retinoschisis." Ophthalmology **115**(4): 718-722.e1.
Jager (1953). "A hereditary retinal disease." Trans Ophthalmol Soc UK **73**: 617–619

Kellner, U., S. Brummer, et al. (1990). "X-linked congenital retinoschisis." Graefes Arch Clin Exp Ophthalmol **228**(5): 432-7.
Kim, L. S., W. Seiple, et al. (2007). "Multifocal ERG findings in carriers of X-linked retinoschisis." Doc Ophthalmol **114**(1): 21-6.
LaVail, M. M., D. Yasumura, et al. (1998). "Protection of mouse photoreceptors by survival factors in retinal degenerations." Invest Ophthalmol Vis Sci **39**(3): 592-602.
Le Meur, G., K. Stieger, et al. (2007). "Restoration of vision in RPE65-deficient Briard dogs using an AAV serotype 4 vector that specifically targets the retinal pigmented epithelium." Gene Ther **14**(4): 292-303.
Lesch, B., V. Szabo, et al. (2008). "Clinical and genetic findings in Hungarian patients with X-linked juvenile retinoschisis." Molecular vision **14**: 2321-32.
Maguire, A. M., F. Simonelli, et al. (2008). "Safety and efficacy of gene transfer for Leber's congenital amaurosis." N Engl J Med **358**(21): 2240-8.
Min, S. H., L. L. Molday, et al. (2005). "Prolonged recovery of retinal structure/function after gene therapy in an Rs1h-deficient mouse model of x-linked juvenile retinoschisis." Mol Ther **12**(4): 644-51.
Narfstrom, K., M. L. Katz, et al. (2003). "Functional and structural recovery of the retina after gene therapy in the RPE65 null mutation dog." Invest Ophthalmol Vis Sci **44**(4): 1663-72.
Newman, E. A. and L. L. Odette (1984). "Model of electroretinogram b-wave generation: a test of the K+ hypothesis." J Neurophysiol **51**(1): 164-82.
Osterberg, G. (1935). Topography of the layer of rods and cones in the human retina, Copenhagen.
Pagenstecher, H. E. (1913). "Über eine unter dem Bilde der Netzhautablösung verlaufende, erbliche Erkrankung der Retina." Graefe's Archive for Clinical and Experimental Ophthalmology **86**(3): 457-462.
Peachey, N. S., G. A. Fishman, et al. (1987). "Psychophysical and electroretinographic findings in X-linked juvenile retinoschisis." Arch Ophthalmol **105**(4): 513-6.
Penn, R. D. and W. A. Hagins (1969). "Signal transmission along retinal rods and the origin of the electroretinographic a-wave." Nature **223**(5202): 201-4.
Pimenides, D., N. D. George, et al. (2005). "X-linked retinoschisis: clinical phenotype and RS1 genotype in 86 UK patients." J Med Genet **42**(6): e35.
Prenner, J. L., A. Capone, Jr., et al. (2006). "CONGENITAL X-LINKED RETINOSCHISIS CLASSIFICATION SYSTEM." Retina **26**(7 SUPPLEMENT): S61-S64.

Regillo, C. D., W. S. Tasman, et al. (1993). "Surgical management of complications associated with X-linked retinoschisis." Arch Ophthalmol **111**(8): 1080-6.
Robson, J. G. and L. J. Frishman (1995). "Inner-retinal components contribute to the a-wave of the ERG of the dark-adapted cat." Vision Research **35**(1000): 71-71.
Rodriguez, F. J., A. Rodriguez, et al. (2005). "X-linked retinoschisis in three females from the same family: a phenotype-genotype correlation." Retina **25**(1): 69-74.
Roesch, M. T., C. C. Ewing, et al. (1998). "The natural history of X-linked retinoschisis." Can J Ophthalmol **33**(3): 149-58.
Rosenfeld, P. J., H. W. Flynn, Jr., et al. (1998). "Outcomes of vitreoretinal surgery in patients with X-linked retinoschisis." Ophthalmic Surg Lasers **29**(3): 190-7.
Saldana, M., J. Thompson, et al. (2007). "X-linked retinoschisis in a female with a heterozygous RS1 missense mutation." Am J Med Genet A **143**(6): 608-9.
Salvetti, A., S. Oreve, et al. (1998). "Factors influencing recombinant adeno-associated virus production." Hum Gene Ther **9**(5): 695-706.
Sasaki, K., H. Ideta, et al. (1995). "Epidemiologic characteristics of rhegmatogenous retinal detachment in Kumamoto, Japan." Graefes Arch Clin Exp Ophthalmol **233**(12): 772-6.
Sauer, C. G., A. Gehrig, et al. (1997). "Positional cloning of the gene associated with X-linked juvenile retinoschisis." Nat Genet **17**(2): 164-70.
Shinoda, K., S. Ishida, et al. (2000). "Clinical characteristics of 14 japanese patients with X-linked juvenile retinoschisis associated with XLRS1 mutation." Ophthalmic Genet **21**(3): 171-80.
Sieving, P. A., E. L. Bingham, et al. (1999). "Juvenile X-linked retinoschisis from XLRS1 Arg213Trp mutation with preservation of the electroretinogram scotopic b-wave." Am J Ophthalmol **128**(2): 179-84.
Sieving, P. A., J. H. Niffenegger, et al. (1986). "Electroretinographic findings in selected pedigrees with choroideremia." American journal of ophthalmology **101**(3): 361.
Stockton, R. A. and M. M. Slaughter (1989). "B-wave of the electroretinogram. A reflection of ON bipolar cell activity." Journal of General Physiology **93**(1): 101.
Sutter, E. E. and D. Tran (1992). "The field topography of ERG components in man--I. The photopic luminance response." Vision Research **32**(3): 433.
Takada, Y., R. N. Fariss, et al. (2006). "Retinoschisin expression and localization in rodent and human pineal and consequences of mouse RS1 gene knockout." Mol Vis **12**: 1108-16.

Takada, Y., R. N. Fariss, et al. (2004). "A retinal neuronal developmental wave of retinoschisin expression begins in ganglion cells during layer formation." Invest Ophthalmol Vis Sci **45**(9): 3302-12.
Takada, Y., C. Vijayasarathy, et al. (2008). "Synaptic pathology in retinoschisis knockout (Rs1-/y) mouse retina and modification by rAAV-Rs1 gene delivery." Invest Ophthalmol Vis Sci **49**(8): 3677-86.
Tantri, A., T. R. Vrabec, et al. (2004). "X-linked retinoschisis: a clinical and molecular genetic review." Surv Ophthalmol **49**(2): 214-30.
The Retinoschisis, C. (1998). "Functional implications of the spectrum of mutations found in 234 cases with X-linked juvenile retinoschisis. The Retinoschisis Consortium." Hum Mol Genet **7**(7): 1185-92.
Verardo, M. R., G. P. Lewis, et al. (2008). "Abnormal reactivity of muller cells after retinal detachment in mice deficient in GFAP and vimentin." Invest Ophthalmol Vis Sci **49**(8): 3659-65.
Veske, A., S. E. Nilsson, et al. (1998). "Retinal dystrophy of Swedish briard/briard-Beagle dogs is due to a 4-bp deletion in the canine RPE65 gene." Am J Hum Genet **63**: A391.
Vogel, W. (1999). "Discoidin domain receptors: structural relations and functional implications." Faseb J **13 Suppl**: S77-82.
Walz, C. M., T. R. Anisi, et al. (1998). "Detection of infectious adeno-associated virus particles in human cervical biopsies." Virology **247**(1): 97-105.
Weber, M., J. Rabinowitz, et al. (2003). "Recombinant adeno-associated virus serotype 4 mediates unique and exclusive long-term transduction of retinal pigmented epithelium in rat, dog, and nonhuman primate after subretinal delivery." Mol Ther **7**(6): 774-81.
Wu, W. W., J. P. Wong, et al. (2005). "RS1, a discoidin domain-containing retinal cell adhesion protein associated with X-linked retinoschisis, exists as a novel disulfide-linked octamer." J Biol Chem **280**(11): 10721-30.
Xu, X. and C. J. Karwoski (1994). "Current source density (CSD) analysis of the ERG d-wave." Invest Ophthalmol Vis Sci.

Other related papers

- Park TK, Wu, **Kjellstrom S**, Zeng Y, Bush R.A, Sieving P.A, Colosi P. (2009). "Intravitreal delivery of AAV8 retinoschisin results in cell type-specific gene expression and retinal rescue in the *Rs1*-KO mouse." *Gene therapy* **16**(7): 916-26

- Haruta M, Bush RA, **Kjellstrom S**, Le Y, Camasamudram V., Sieving P.A. Depleting Rac1 component of NADPH oxidase in mouse photoreceptors protects from photo-oxidative stress without affecting rod structure. *Proc Natl Acad Sci U S A* **106**(23): 9397-402.

- Takada, Y., Vijayasarathy, C., Zeng, Y., **Kjellstrom, S**., Bush, R.A., Sieving, P.A Synaptic pathology in retinoschisis knockout (Rs -/y) mouse retina and modification by rAAV-Rs1 gene delivery. *Investigative ophthalmology & visual science.* 2008 Aug;49(8):3677

- Brooks B.P, Larson D.M, Chan C.C, **Kjellstrom S**, Smith R.S, Crawford M.A, Lamoreux L, Huizing M, Hess R, Jiao X, Hejtmancik J.F, Maminishkis A, John S.W, Bush R.A, Pavan W.J. Analysis of ocular hypopigmentation in Rab38cht/cht mice. *Invest Ophthalmol Vis Sci.* 2007 Sep;48(9):3905-13.

- Wen R, Song Y, **Kjellstrom S**, Tanikawa A, Liu Y, Li Y, Zhao L, Bush R.A, Laties AM, Sieving PA. Regulation of rod phototransduction machinery by ciliary neurotrophic factor. *J Neurosci.* 2006 Dec 27;26(52):13523-30.

- Haywood-Watson R.J, Ahmed Z.M, **Kjellstrom S (shared 1st author),** Bush R.A, Takada Y, Hampton L.L, Battey J.F, Sieving P.A, Friedman T.B. Ames Waltzer deaf mice have reduced electroretinogram amplitudes and complex alternative splicing of Pcdh15 transcripts. *Invest Ophthalmol Vis Sci.* 2006 Jul;47(7):3074-84.

Appendices